



## Variability of earthquake nucleation in continuum models of rate-and-state faults and implications for aftershock rates

Y. Kaneko<sup>1</sup> and N. Lapusta<sup>1,2</sup>

Received 4 May 2007; revised 17 August 2008; accepted 9 September 2008; published 31 December 2008.

[1] Using two continuum models of rate-and-state faults, one with a weaker patch and the other with rheological transition from steady state velocity-weakening to velocity-strengthening friction, we simulate several scenarios of spontaneous earthquake nucleation plausible for natural faults, investigate their response to static shear stress steps, and infer the corresponding aftershock rates. Overall, nucleation processes at weaker patches behave similarly to theories based on spring-slider models, with some notable deviations. In particular, nucleation and aftershock rates are affected by normal stress heterogeneity in the nucleation zone. Nucleation processes at rheological transitions behave differently, producing complex slip velocity histories, nonmonotonic responses to static stress changes, and aftershock rates with pronounced peaks and seismic quiescence. For such processes, positive stress steps sometimes delay nucleation of seismic events by inducing aseismic transients that relieve stress and postpone seismic slip. Superposition of the complex aftershock response for spatially variable stress changes results in Omori's law for a period of time followed by seismic quiescence. Such behavior was observed at the base of the seismogenic zone near the 1984 Morgan Hill earthquake. We show that the computed aftershock rates are linked to unperturbed slip velocity evolution in the nucleation zone and construct simplified analytical scenarios that explain some features of the response. The qualitative differences that we find between the two nucleation models indicate that aftershock response of rate-and-state faults to static stress changes would depend on the conditions under which nucleation occurs on natural faults and may be different from predictions based on spring-slider models.

**Citation:** Kaneko, Y., and N. Lapusta (2008), Variability of earthquake nucleation in continuum models of rate-and-state faults and implications for aftershock rates, *J. Geophys. Res.*, 113, B12312, doi:10.1029/2007JB005154.

### 1. Introduction

[2] Understanding earthquake nucleation is an important yet difficult task due to lack of direct observations such as in situ measurements at seismogenic depths. A widely accepted model for earthquake nucleation is a developing frictional instability on a preexisting fault, the phenomenon inferred from laboratory experiments and theoretical studies. In this work, we simulate, in the context of earthquake sequences, several plausible scenarios of earthquake nucleation on faults embedded in an elastic medium and governed by rate- and state-dependent friction. We then explore variability in simulated earthquake nucleation due to fault heterogeneities and different loading conditions and study implications for aftershock occurrence.

[3] The rate-and-state friction laws we adopt have been developed on the basis of laboratory rock experiments [e.g., Dieterich, 1978, 1979; Ruina, 1983; Tullis, 1988; Blanpied *et al.*, 1995; Marone, 1998] for slip velocities from  $10^{-8}$  to  $10^{-3}$  m/s, the range of particular relevance to earthquake nucleation. The laws have been successfully used to model and explain various earthquake phenomena including earthquake nucleation, postseismic slip, foreshocks, aftershocks, and aseismic transients [e.g., Rice and Ruina, 1983; Ruina, 1983; Marone *et al.*, 1991; Dieterich, 1992, 1994; Tullis, 1996; Ben-Zion and Rice, 1997; Gombert *et al.*, 1998; Marone, 1998; Lapusta and Rice, 2003; Perfettini *et al.*, 2003; Liu and Rice, 2005; Miyazaki *et al.*, 2006]. In the standard aging formulation for situations with time-independent effective normal stress  $\bar{\sigma}$ , the shear strength  $\tau$  is expressed as

$$\tau = \bar{\sigma}\mu = \bar{\sigma} \left[ \mu_0 + a \ln \left( \frac{V}{V_0} \right) + b \ln \left( \frac{V_0 \theta}{L} \right) \right] \quad (1)$$

$$\frac{d\theta}{dt} = 1 - \frac{V\theta}{L}, \quad (2)$$

<sup>1</sup>Division of Geological and Planetary Sciences, California Institute of Technology, Pasadena, California, USA.

<sup>2</sup>Also at Division of Engineering and Applied Science, California Institute of Technology, Pasadena, California, USA.

where  $a > 0$  and  $b > 0$  are rate-and-state constitutive parameters,  $V$  is slip velocity,  $\mu_0$  is the reference friction coefficient corresponding to the reference slip velocity  $V_0$ ,  $\theta$  is a state variable which can be interpreted as the average age of the population of contacts between two surfaces, and  $L$  is the characteristic slip for state evolution [e.g., *Dieterich*, 1978, 1979; *Rice and Ruina*, 1983; *Ruina*, 1983; *Dieterich and Kilgore*, 1994]. Note that other equations for state-variable evolution and formulations with two and more state variables have been proposed [*Ruina*, 1983; *Rice and Ruina*, 1983; *Gu et al.*, 1984; *Kato and Tullis*, 2001]. Recent studies rekindled the discussion of which state evolution laws are more appropriate to use in earthquake modeling. *Bayart et al.* [2006] showed that the so-called “slip” form of the evolution equation provides a better match to velocity jump experiments. Studies of aftershock rates based on spring-slider models [*Gomberg et al.*, 2000] and a recent nucleation study [*Ampuero and Rubin*, 2008] found notable differences between models with the aging law and models with the slip law. We discuss the applicability of our results to other rate-and-state formulations in section 9.

[4] Stability of sliding and nucleation of seismic slip on rate-and-state faults governed by laws (1) and (2) have been considered in a number of theoretical studies [*Rice and Ruina*, 1983; *Ruina*, 1983; *Dieterich*, 1992; *Rice et al.*, 2001; *Rubin and Ampuero*, 2005]. Fault regions with  $a - b > 0$  have steady state velocity-strengthening friction properties and tend to slip in a stable manner with the imposed loading rate. Fault regions with  $a - b < 0$  have steady state velocity-weakening properties and are capable of producing earthquakes. However, even on steady state velocity-weakening fault regions, sufficiently small slipping zones cannot develop fast slip under slow tectonic loading, and the slipping zone has to become large enough to produce a rapid sliding event. The aseismic process of slow and gradually accelerating slip in a small, slowly varying zone that eventually leads to unstable slip is often referred to as a nucleation process. The term “unstable slip” typically refers to simulated earthquakes that are inertially controlled events characterized by rapid expansion of the slipping zone with rupture speeds that are a significant fraction of wave speeds and slip velocities much larger than the loading rate.

[5] Studies of earthquake nucleation have concentrated on two theoretically interesting and practically important topics: the nucleation size, i.e., the size of the slipping zone right before an earthquake, and implications of nucleation for aftershock phenomena. Several theoretical estimates  $h_{\text{nucl}}$  of the nucleation size have been proposed, all of them in the form

$$h_{\text{nucl}} = \frac{\eta GL}{\bar{\sigma} F}, \quad (3)$$

where  $\eta$  is a model-dependent parameter of order one,  $G$  is the shear modulus, and  $F$  is a function of rate-and-state parameters  $a$  and  $b$ . *Rice and Ruina* [1983], *Ruina* [1983], and *Rice et al.* [2001] considered linear stability of perturbations from steady state sliding and determined that  $F = b - a$ . *Dieterich* [1992] assumed that nucleation processes accelerate fast enough for  $V\theta/L \gg 1$  to hold and obtained  $F = b$ . The estimate of *Dieterich* [1992] was

later confirmed in meter-scale rock friction experiments [*Dieterich and Kilgore*, 1996]. *Rubin and Ampuero* [2005] proposed that there are two regimes controlled by the ratio  $a/b$ . If  $a/b \lesssim 0.37$ , the nucleation proceeds in a fixed region of the size given by (3) with  $F = b$ , as in the estimate by *Dieterich* [1992]. If  $a/b \gtrsim 0.5$ , the nucleation process resembles an expanding crack and the nucleation size asymptotically approaches (3) with  $F = (b - a)^2/b$ . Note that all three estimates match, within factors of order 1, for  $a \ll b$  which implies  $b - a \approx b$ . For  $a$  approaching  $b$  (friction properties close to velocity neutral), both Rice-Ruina and Rubin-Ampuero estimates predict increasingly larger nucleation sizes (although Rubin-Ampuero estimate increases significantly faster). This is consistent with the fact that velocity-strengthening regions cannot spontaneously produce unstable sliding and hence the nucleation size for  $a \geq b$  can be considered infinite.

[6] The second thrust in studying nucleation processes has been motivated by aftershock occurrence. The decay of aftershocks is well described empirically by Omori’s law (see *Utsu et al.* [1995] for a recent review). *Dieterich* [1994] built an aftershock model that reproduced Omori’s law using static triggering of rate-and-state nucleation sites. In that model, a preexisting population of rate-and-state nucleation sites is perturbed by static stress changes due to a main shock. In the population, each nucleation site is governed by the same nucleation process but time shifted in such a way that the population results in a constant background seismicity rate. After a positive static shear stress step, the nucleation process at each site accelerates, producing an increased seismicity rate (or aftershock rate) that matches Omori’s law for a wide range of parameters. An important ingredient in this aftershock model is the nucleation process and its response to static stress changes. *Dieterich* [1994] specified the nucleation process in terms of its slip velocity evolution. To obtain the evolution, two simplifications in modeling nucleation were used: (1) elastic interactions were described by a one-degree-of-freedom spring-slider system and (2) the assumption  $V\theta/L \gg 1$  was used to simplify the rate-and-state friction formulation based on a study of earthquake nucleation in a continuum model [*Dieterich*, 1992]. These simplifications allowed the derivation of analytical expressions for both slip velocity evolution during nucleation and the resulting aftershock rate (Appendix B). The approach of *Dieterich* [1994] has been further explored in a number of works [*Gomberg et al.*, 1998, 2000; *Gomberg*, 2001; *Gomberg et al.*, 2005] and has been used to interpret observed aftershock sequences [*Gross and Kisslinger*, 1997; *Gross and Burgmann*, 1998; *Toda et al.*, 1998, 2005]. In particular, aftershock rates based on simulations in spring-slider systems with the full aging rate-and-state formulation were found to follow the results of *Dieterich* [1994] quite well, validating simplification (2) for spring-slider models.

[7] Given the determining role of the nucleation process in the aftershock model of *Dieterich* [1994] and subsequent studies, it is important to understand whether spring-slider models provide a good approximation of the nucleation process on natural faults. Spring-slider models approximate a slip zone of a constant size (inversely proportional to the spring stiffness assumed) with uniform slip and stress history throughout the slip zone and simplified elastic

interaction with the surrounding bulk. Hence spring-slider models cannot represent spatially inhomogeneous aseismic slip in a zone of evolving size which is a characteristic feature of nucleation processes in models that incorporate both rate-and-state friction laws and elastic continuum [Rice, 1993; Lapusta and Rice, 2002, 2003; Rubin and Ampuero, 2005].

[8] In this study, we simulate and compare several plausible scenarios of earthquake nucleation in continuum models of rate-and-state faults. Two fault models are used to create two different environments for earthquake nucleation. The first model incorporates uniform steady state velocity-weakening friction properties and a weaker patch of slightly (10%) lower effective normal stress. By varying the size of the weaker patch, we can either achieve completely homogeneous fault properties within the nucleation zone or induce normal stress heterogeneity there. This is a realistic nucleation scenario, as faults can contain such weaker patches for a number of reasons that include local fault nonplanarity or spatial variations in pore pressure. At the same time, observations suggest that earthquakes tend to cluster at inferred transitions from locked to creeping regions [e.g., Schaff *et al.*, 2002; Waldhauser *et al.*, 2004]. We explore that scenario in the second model that contains a rheological transition from steady state velocity-strengthening to steady state velocity-weakening friction. Such transitions create stress concentrations that promote earthquake nucleation.

[9] Nucleation processes in this work are simulated as a part of spontaneously occurring earthquake sequences on a fault that is subjected to slow, tectonic-like loading [Lapusta *et al.*, 2000]. This approach allows us to study nucleation processes that naturally develop in our models, with conditions before the nucleation originating from the previous stages of earthquake occurrence and not from arbitrarily selected initial conditions that one would need to impose to study only one instance of earthquake nucleation. Our simulations resolve all stages of each earthquake episode: the aseismic nucleation process in gradually varying zones of accelerating slip, the subsequent inertially controlled event (unstable slip) with realistic slip velocities and rupture speeds, the postseismic slip, and the interseismic quasi-static deformation between events.

[10] We consider five representative cases of earthquake nucleation, compare them in terms of their slip velocity evolution, and discuss the effects of heterogeneity in normal stress, heterogeneity in friction properties, and variations in loading (sections 3 and 4). We find significant differences among the simulated nucleation processes. Since their spatial extent varies with time and their slip and slip velocity vary with space, it is not obvious how to make the direct comparison of the nucleation processes obtained in this work with the ones in spring-slider models. To facilitate such comparison, we study the response of the simulated nucleation processes to static stress changes and the resulting aftershock rates, compare them with the results of Dieterich [1994], and explain the observed similarities and differences (sections 5–8). Overall, the model with a weaker patch behaves similarly to the spring-slider model of Dieterich [1994], while the model with rheological transition exhibits qualitatively different behavior. We summarize our results and discuss their implications in section 9.

[11] In computing the aftershock rates, we assume, following previous approaches [Dieterich, 1994; Gomberg *et al.*, 2000; Gomberg, 2001], that the aftershock-producing nucleation sites are all governed by the same nucleation process, albeit time shifted for each nucleation site. On natural faults, different nucleation sites may have different friction properties, stress conditions, stressing rates, etc. and one would need to consider, in general, a combination of nucleation models of the kind studied in this work to make meaningful comparisons with aftershock observations. Our results on aftershock rates may be useful for explaining observations in special cases, as we show in section 6 for a cluster of aftershocks located at rheological transition. However, the main purpose of the study is to determine whether the response of rate-and-state faults to static stress perturbations changes if one uses models of faults in elastic continuum rather than spring-slider models.

[12] A number of other mechanisms have been proposed to explain aftershock occurrence. These include increased loading rate due to aseismic processes such as postseismic slip [e.g., Benioff, 1951; Perfettini and Avouac, 2004] or relaxation of the viscoelastic lower crust [e.g., Freed and Lin 2001], pore fluid motion and induced variations in fault strength [e.g., Nur and Booker, 1972; Bosl and Nur, 2002], triggering due to dynamic stress changes [e.g., Hill *et al.*, 1993; Gomberg *et al.*, 2003; Felzer and Brodsky, 2006], and evolution of viscoelastic damage rheology due to sudden increase in strain [e.g., Ben-Zion and Lyakhovsky 2006]. The full explanation for aftershocks may involve a combination of several mechanisms, with different mechanisms potentially dominating in different situations or during different stages of aftershock sequences. However, it becomes increasingly clear that rate-and-state friction is a good description of the fault constitutive response during slow slip, and hence accelerated rate-and-state nucleation due to static stress changes has the potential to significantly contribute to all aftershock sequences. Our study of this aftershock-producing mechanism with continuum models of earthquake nucleation is a useful first step toward understanding the combined effects of several mechanisms as discussed in section 9.

## 2. Two-Dimensional Continuum Models of Earthquake Nucleation

[13] We consider earthquake nucleation on a planar fault embedded into an elastic medium of homogeneous elastic properties with the shear wave speed  $c_s = 3.0$  km/s, shear modulus  $G = 30$  GPa, and Poisson's ratio  $\nu = 0.25$ . On the fault, a potentially seismogenic patch borders regions steadily moving with a prescribed slip rate  $V_L = 1$  mm/a, as illustrated in Figure 1a. That steady motion provides loading in our models. The loading slip rate  $V_L = 1$  mm/a is on the low end of typical plate rates but it could be representative of steady slip achieved locally on faults, especially in the case of secondary faults or multiple fault strands. The fault resistance to sliding is given by rate-and-state friction regularized at zero slip velocity [Rice and Ben-Zion, 1996; Lapusta *et al.*, 2000]. The value of characteristic slip  $L$  in simulations presented in this work is  $80 \mu\text{m}$  (unless noted otherwise), as laboratory-like values of  $L$  (of order  $1 - 100 \mu\text{m}$ ) are required to account for the presence of

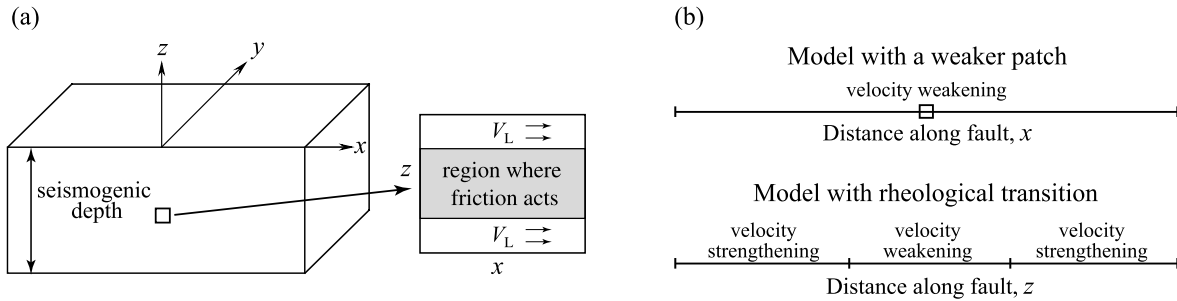


**Figure 1.** (a) Three-dimensional schematics of a planar fault in an elastic medium. This study employs simplified 2-D models and focuses on a small region indicated by the square. The fault region governed by rate-and-state friction (shown in gray) is loaded by relative motion above and below the region with a prescribed slip rate  $V_L$ . (b) Schematics of fault properties in the simplified 2-D continuum models. (top) In the model with a weaker patch, the fault has steady state velocity-weakening properties everywhere and contains a patch of lower effective normal stress indicated by a square. (bottom) In the model with rheological transition, a steady state velocity-weakening region is surrounded by steady state velocity-strengthening regions.

small ( $M \sim 0$ ) earthquakes on natural faults [e.g., *Lapusta and Rice, 2003*].

[14] Two simplified fault models that we use to create two conceptually different scenarios of earthquake nucleation are described in sections 2.1–2.2 and illustrated in Figure 1b. More details are given in Appendix A. The friction and stress parameters of the models are summarized in Table 1 and Figure 2. To simulate spontaneous slip accumulation in terms of earthquake sequences, we use the boundary integral method developed by *Lapusta et al. [2000]* and *Lapusta [2001]*.

### 2.1. Model With a Weaker Patch

[15] The first model incorporates a weaker patch of 10% lower effective normal stress. The model is based on the crustal plane model [*Lapusta, 2001*]; it restricts the fault to motions parallel to the along-strike direction  $x$ , eliminates the fault depth by considering depth-averaged quantities, and retains variations only in the along-strike direction  $x$ . These modifications turn the 2-D planar fault into a 1-D along-strike analog (Figure 1b), with the fault behavior described by strike-parallel slip  $\delta(x, t)$ , slip velocity (or slip rate)  $V(x, t) = \partial\delta(x, t)/\partial t$ , and the relevant component of shear stress  $\tau(x, t)$ . Compressive effective normal stress  $\bar{\sigma}(x)$  does not depend on time in the cases considered in this work. At the ends of the fault, there are zones of zero initial shear stress to stop dynamic events (Figure 2). Hence the extent of the fault capable of sustaining dynamic events is 1000 m. A more physical approach would be to replace the zero-stress regions with regions of velocity-strengthening properties, but that would create alternative places for earthquakes to nucleate, and in this model we would like to avoid such complexities. By making earthquakes nucleate in the designated place, i.e., at the weaker patch in the middle of the fault, we can control how heterogeneous the imposed conditions are in the nucleation region.

[16] We have done a number of simulations of earthquake sequences in this model, varying the values of parameters  $a$  (0.0015–0.015),  $b$  (0.0055–0.019),  $L$  (10–120  $\mu\text{m}$ ), and the size of the weaker patch (2–200 m). We present results for three representative cases, all with  $L = 80 \mu\text{m}$ .

[17] In case 1, the size of the weaker patch, 100 m, is much larger than the nucleation size, which is less than 30 m in this case. Hence there is no imposed heterogeneity within the nucleation zone. Values  $a = 0.015$  and  $b = 0.019$  are used (Figure 2), which are typical of laboratory experiments. Nucleation proceeds under stress conditions that are relatively homogeneous compared to other cases. However, in this and all other cases, shear stress concentrations do develop, as expected, at the edges of the slowly varying zone of faster slip.

[18] In case 2, the size of the weaker patch, 10 m, is a significant fraction of the nucleation zone that develops. Nucleation proceeds under imposed conditions of heterogeneous normal stress within the nucleation zone. The other parameters are the same as in case 1.

[19] In case 3, the value of  $a = 0.0015$  is 10 times smaller than that of cases 1 and 2. This value is representative of the ones inferred from aftershock observations based on the model of *Dieterich [1994]*, assuming overburden normal stress minus hydrostatic pore pressure [*Gross and Kisslinger, 1997; Gross and Burgmann, 1998; Toda et al., 1998, 2005*]. The parameter  $b = 0.0055$  is chosen to keep  $(b - a)$  the same as in cases 1 and 2, ensuring the same steady state velocity-weakening properties. The size of the weaker region, 10 m, is a significant fraction of the nucleation zone, as in case 2. Note that the ratio  $a/b$  is 0.27 in this case, while  $a/b = 0.79$  for cases 1 and 2. According to the study of *Rubin and*

**Table 1.** Friction-Related Parameters of Both Models

Parameter	Symbol	Value
Reference slip velocity	$V_0$	$10^{-6}$ m/s
Reference friction coefficient	$\mu_0$	0.6
Characteristic slip distance	$L$	80.0 $\mu\text{m}$
Effective normal stress	$\bar{\sigma}$	50.0 MPa <sup>a</sup>
Rate-and-state parameter $a$	$a$	0.015 or 0.0015 <sup>b</sup>
Rate-and-state parameter $b$	$b$	0.019 or 0.0055 <sup>b</sup>

<sup>a</sup>In the model with a weaker patch,  $\bar{\sigma} = 50$  MPa in the patch and  $\bar{\sigma} = 55.6$  MPa outside the patch.

<sup>b</sup>The indicated values of  $a$  and  $b$  are valid for the entire fault in the model with a weaker patch and for the part of the steady state velocity-weakening region of the model with rheological transition where  $a$  and  $b$  are constant.

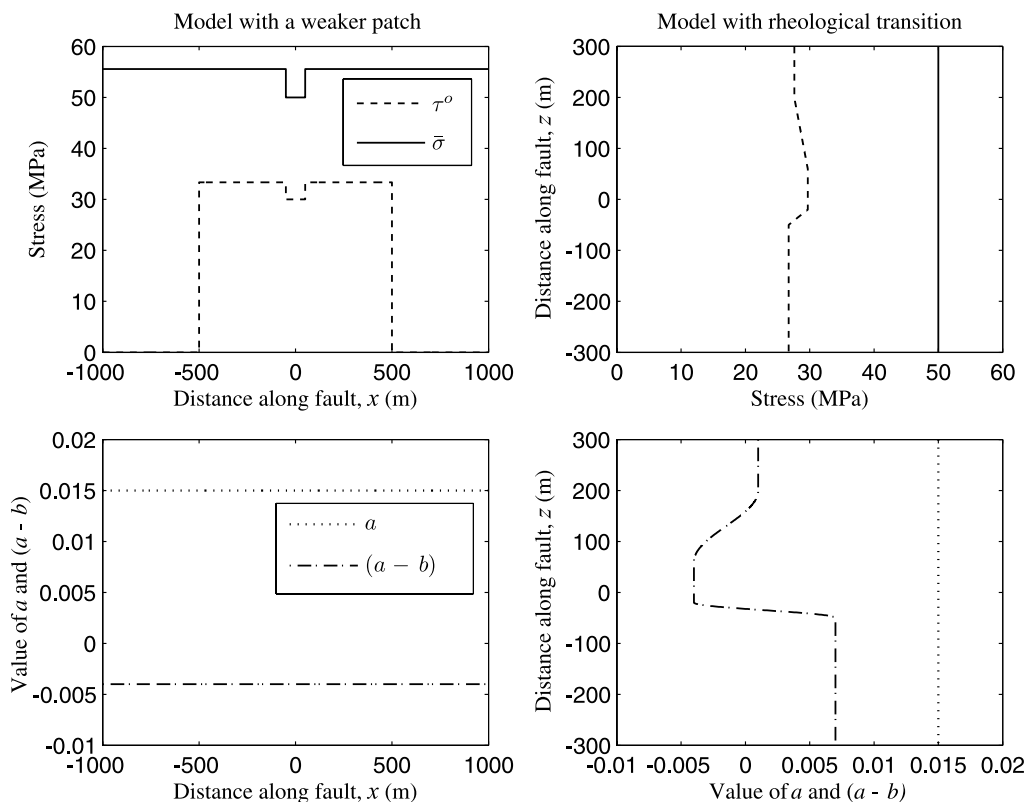


**Figure 2.** (top) Distributions of effective normal stress  $\bar{\sigma}$  and initial shear stress  $\tau^o$  in the two models. In the model with a weaker patch, the region of lower  $\bar{\sigma}$  is introduced in the middle of the fault to encourage earthquake nucleation there. The size of the weaker region varies in different cases studied. (bottom) Examples of distributions of rate-and-state parameters  $a$  and  $(a - b)$  in the two models. Locations with  $a - b = 0$  correspond to rheological transitions from velocity-weakening to velocity-strengthening steady state friction. We vary  $a$  and  $b$  in the presented cases but keep  $(a - b)$  the same in all cases.

*Ampuero* [2005], this represents a qualitative difference, as explained in section 1.

## 2.2. Model With Rheological Transition

[20] The second model contains variations in steady state friction properties that create rheological transitions. It is analogous to the depth-variable model of *Lapusta et al.* [2000]. The fault motion is still in the along-strike direction  $x$ , but only variations with depth  $z$  are considered, so that the fault behavior is described by strike-parallel slip  $\delta(z, t)$ , slip velocity (or slip rate)  $V(z, t) = \partial\delta(z, t)/\partial t$ , and the relevant component of shear stress  $\tau(z, t)$ . Unlike the model studied by *Lapusta et al.* [2000], the model in this work does not include the free surface. The effective normal stress  $\bar{\sigma}$  is constant along the entire fault (Figure 2).

[21] We have done a number of simulations in this model, varying the values of  $a$  and  $b$  in the velocity-weakening region (0.0015–0.015 and 0.0055–0.023, respectively) and  $L$  (20–160  $\mu\text{m}$ ). We present results for two representative cases, both with  $L = 80 \mu\text{m}$ .

[22] In case 4,  $a = 0.015$  and  $b = 0.019$  in the steady state velocity-weakening region, as in cases 1 and 2 of the model with a weaker patch. Full distributions of  $a$  and  $b$  are shown in Figure 2. This variation is qualitatively similar to the one in *Rice* [1993] and *Lapusta et al.* [2000]. The distributions of  $a$  and  $b$  are asymmetric with respect to the middle of the

fault, so that simulated earthquakes nucleate at one of the rheological transitions.

[23] In case 5,  $a = 0.0015$  and  $b = 0.0055$  in the steady state velocity-weakening region, as in case 3. Throughout the fault domain, this case has 10 times smaller  $a$  than case 4 and such  $b$  that the distribution of  $(a - b)$  is the same in both cases. The same distribution of  $(a - b)$  ensures that rheological transitions are at the same locations in both cases.

## 3. Simulated Nucleation Processes

### 3.1. Nucleation Processes due to Weaker Patches and Importance of Normal Stress Heterogeneity

[24] As an example of fault slip simulated in the model with a weaker patch, consider the earthquake sequence for case 1 (Figure 3a). Earthquakes nucleate in the middle of the fault, due to the weaker patch. The earthquakes then spread bilaterally along the strike of the fault; the dashed lines show slip accumulation every 0.01 s during the dynamic rupture. When the rupture reaches zero-stress barriers, it arrests. The interseismic period is 28 years. We take the nucleation process of the third event as the representative one for this case; the corresponding part in Figure 3 is surrounded by a small rectangle.

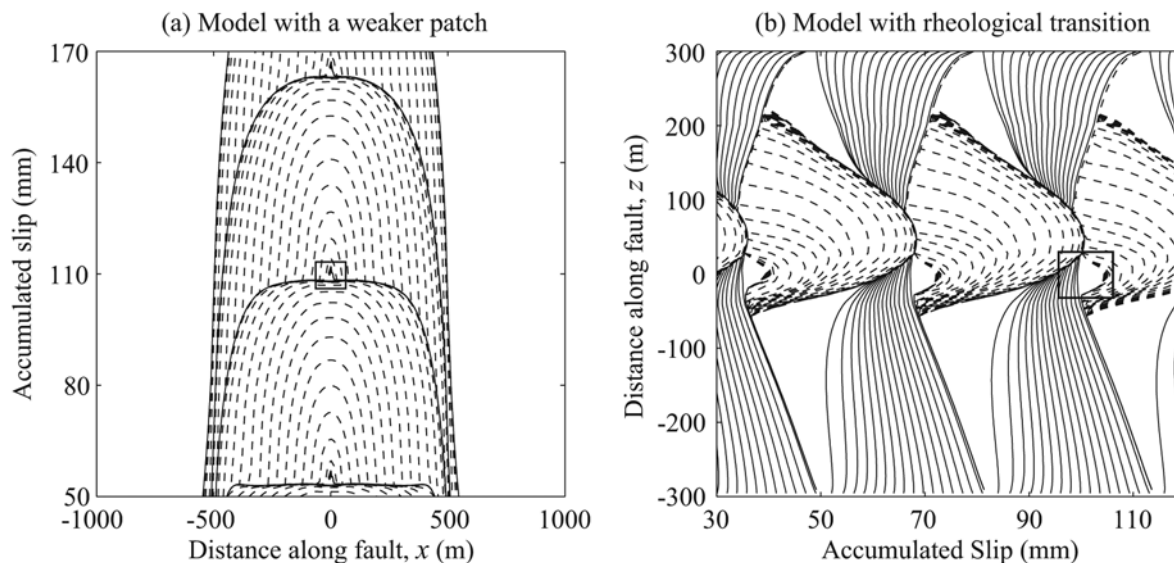


**Figure 3.** Examples of earthquake sequences simulated (a) in the model with a weaker patch and (b) in the model with rheological transition. Solid lines show slip accumulation every 2 years. Dashed lines are intended to capture dynamic events and are plotted every 0.01 s during the simulated earthquakes. For each earthquake, the dashed lines are shown from 0.05 s before our definition of the onset of an earthquake (rupture speed reaching 10% of the shear wave speed) until the maximum slip velocity on the fault reduces to 1 mm/s. The nucleation process of a representative earthquake is indicated by a rectangle.

[25] To study nucleation sizes and aftershock rates, we need to define when the nucleation process ends and the dynamic event begins. *Dieterich* [1992, 1994] used quasi-static equations, and their solution ceased to exist (i.e., slip velocities became infinite) when inertial effects would have been important in the complete formulation. The time at which the solution ceased to exist was taken as the time of instability onset. Since our simulations fully account for inertial effects and capture the smooth transition between the quasi-static phase and dynamic rupture, defining the beginning of an earthquake is not so simple. We use the criterion based on rupture speed and take, as the onset of instability, the time at which a tip of the actively slipping zone moves with the speed that exceeds a fraction (10%) of the shear wave speed of the surrounding elastic medium. The tips of the actively slipping zone are found as the locations of shear stress concentration. The sliding region changes very slowly in space during the quasi-static deformation, and extends with rupture speeds comparable to the shear wave speed during the dynamic phase. Hence this rupture definition allows us to appropriately capture the transition. An alternative approach would be to define the beginning of an earthquake as the time when slip velocities reach a certain value, e.g., 0.1 m/s, either at a particular location or as a maximum on the fault. Note that the two criteria are related, as faster slip velocities correspond to larger rupture speeds.

[26] Representative nucleation processes for cases 1–3 are shown in Figure 4. The dashed lines in Figures 4a–4c show slip accumulation every 0.01 s starting with 0.05 s before our definition of the beginning of an earthquake. The first five dashed lines are almost on top of each other, signifying still relatively slow slip and slow expansion of

the sliding region. The sixth line shows much faster slip and expansion, indicating the beginning of a dynamic event. Figures 4d–4f illustrate the imposed distribution of effective normal stress and the approximate extent of the spontaneous nucleation zone.

[27] The comparison of cases 1 and 2 shows an interesting result. The presence of slight normal stress heterogeneity within the nucleation zone in case 2 leads to 1.5 times larger nucleation size for that case, 36 m versus 24 m for case 1. Average normal stress is larger in case 2, with all other parameters being the same, and all existing estimates of earthquake nucleation sizes discussed in section 1 would predict that the nucleation size should be smaller in case 2 than in case 1, but the opposite is observed. The antiplane estimate of nucleation size by *Rubin and Ampuero* [2005] gives 36 m for the parameters of these cases. Since we use a depth-averaged model, the direction  $x$  is affected by a factor of  $Z = 1/(1 - \nu) = 4/3$  (Appendix A) and hence the estimate becomes 48 m. This is broadly consistent with the nucleation sizes in cases 1 and 2, in the sense that the estimate gives a close upper bound. Note that the energy balance in the expanding crack solution of *Rubin and Ampuero* [2005], when adopted to the normal-stress heterogeneity of case 2, would be qualitatively consistent with the larger nucleation size for case 2 (A. Rubin, personal communication, 2007). This result demonstrates that stress heterogeneities on faults can have significant, and sometimes counterintuitive, effect on nucleation processes.

[28] Case 3, with a smaller value of  $a/b$ , behaves differently from cases 1 and 2. The nucleation size in case 3 is about 29 m. We simulated a number of cases similar to case 3 but with different sizes of the weaker patch, including the case in which the weaker patch was much larger than the

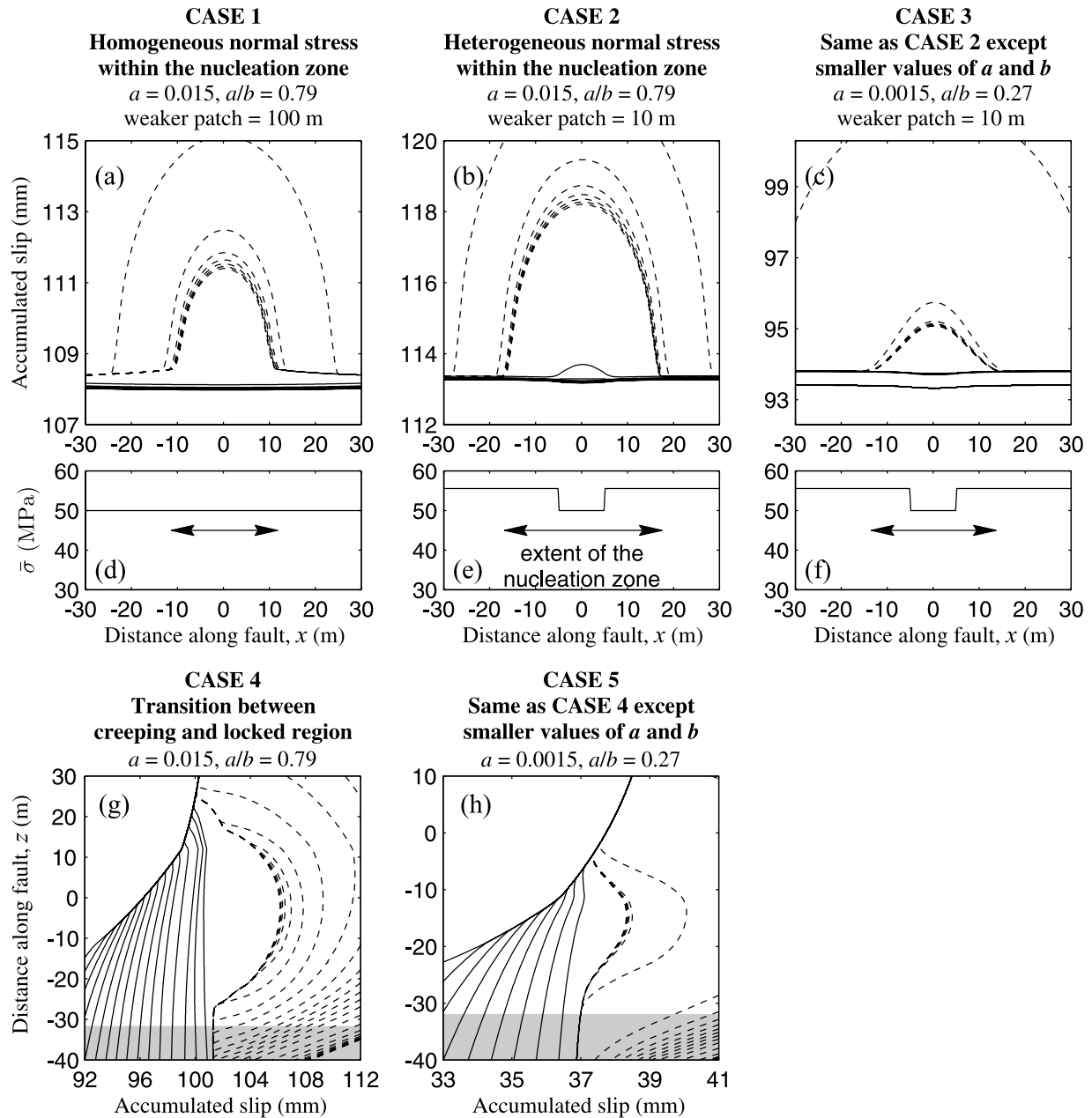


**Figure 4.** (a–c) Nucleation processes at weaker patches. Cases 1–3 correspond to either different sizes of the weaker patch or different constitutive parameters  $a$  and  $b$ . The other parameters are the same for all three cases. (d–f) Distribution of effective normal stress  $\bar{\sigma}$  in a region that includes the nucleation zone. Double arrows indicate the extent of the nucleation zone for each case. (g–h) Nucleation processes at rheological transition. Cases 4 and 5 correspond to different constitutive parameters  $a$  and  $b$ . Solid and dashed lines in Figures 4a–4c and 4g–4h have the same meaning as in Figure 3. Shaded areas correspond to velocity-strengthening regions.

resulting nucleation size. In all those cases, the nucleation size changed very little compared to case 3. This means that the effect of heterogeneity on the nucleation size is diminished for sufficiently small values of  $a/b$ . We also find that smaller values of  $a/b$  lead to shorter periods of interseismic deformation between two successive earthquakes. In case 3, the interseismic period is 23.8 years, smaller than the interseismic period of 29.1 years in case 2, despite the fact that  $(b - a)$  is the same in the two cases.

### 3.2. Nucleation Processes due to Rheological Transitions

[29] An earthquake sequence simulated in the model with rheological transition is shown in Figure 3b, using case 4 as an example. The solid lines are plotted every 2 years and show the continuous slow sliding (creep) of the steady state velocity-strengthening regions. That slow slip creates stress concentration at its tip and penetrates into the velocity-weakening region. In due time, an earthquake nucleates

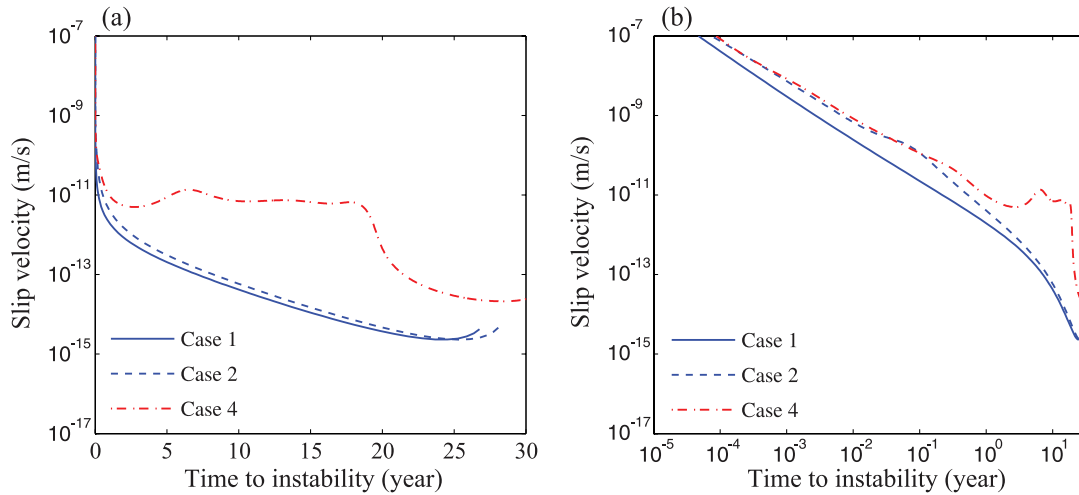


**Figure 5.** Slip velocity evolution during one earthquake cycle for representative points inside nucleation zones on (a) linear and (b) logarithmic timescales. Time to instability  $T$  is given by  $T = t_2 - t$ ,  $t_1 < t < t_2$ , where  $t_1$  and  $t_2$  are the occurrence times of two consecutive earthquakes in years. For each case, slip velocity for times  $t_1 + 1 < t < t_2$  is shown. Slip velocity at  $x = 0$  km is plotted for cases 1 and 2, and slip velocity at  $z = 0$  is plotted for case 4. Note that slip velocity evolution for nucleation processes at rheological transition is nonmonotonic.

close to the transition; its progression is shown by dashes lines. After an earthquake arrests, the velocity-strengthening region experiences accelerated sliding, or afterslip, due to the transferred stress. The interseismic period between two successive events is 32 years. We take the nucleation process of the fourth event as the representative one for this case; the relevant part of Figure 3 is surrounded by a small rectangle.

[30] Representative nucleation processes for cases 4 and 5 are shown in Figure 4. Nucleation of the simulated earthquakes occurs within the velocity-weakening region, but close to transition to velocity-strengthening friction (Figures 4g and 4h; the transition is at  $z = -32$  m in both cases). Because of interactions with the nearby creeping region, such nucleation proceeds under temporally and spatially nonuniform stress field. The different values for  $a - b$  (with the same value of  $b - a$ ) in cases 4 and 5 lead to notable differences in nucleation processes. The nucleation sizes in cases 4 and 5 are different and approximately consistent with the estimates of *Rubin and Ampuero* [2005], which are  $2\mu Lb/(\pi\bar{\sigma}(b - a)^2) = 36$  m for case 4 and  $2.74\mu L/(\bar{\sigma}b) = 24$  m for case 5. Note that *Rubin and Ampuero* [2005] gave formulae for half of the nucleation size but we use full nucleation sizes here. In our simulations, the nucleation sizes are 35 to 40 m for case 4 and 18 to 24 m for case 5, as can be estimated from Figure 4.

[31] As in the model with a weaker patch, smaller values of  $a/b$  result in shorter interseismic periods, but the effect is much stronger in the model with rheological transition. In case 5, the interseismic period is 18 years, almost twice shorter than the interseismic period of 32 years in case 4. In the model with a weaker patch, the interseismic period is dictated by the loading time necessary to rebuild the stress relieved during a dynamic event and hence depends on the static stress drop, which is similar in cases 1 and 3. In the model with rheological transition, the interseismic period is controlled by the time it takes for the slow slip penetrating

from the velocity-strengthening region to create a slipping zone comparable to the nucleation size. Since the nucleation size is almost twice smaller in case 5 than in case 4, the interseismic period is also almost twice smaller.

### 3.3. Different Time Evolution of Nucleation in the Two Models

[32] The nucleation sizes in both models are comparable for a given set of rate-and-state parameters (Figure 4). The question arises whether the time evolution of the nucleation processes in the two models is also similar. In Figure 5, we compare slip-velocity evolution for representative points inside the nucleation zones at weaker patches (cases 1 and 2) and at rheological transitions (case 4). In the model with a weaker patch, slip velocity gradually increases through the interseismic period, and this behavior is qualitatively consistent with that of spring-slider models [*Dieterich*, 1994; *Gomberg et al.*, 2000]. Still, slip velocity in cases 1 and 2 is slightly different, especially for the period from  $10^{-3}$  to  $10^0$  years before an earthquake (Figure 5b). This can only be caused by normal-stress heterogeneity within the nucleation zone, as this is the only difference between cases 1 and 2. Nucleation in the model with rheological transition (case 4) is significantly different: slip velocity increases first, then stays relatively constant for about 20 years, with some oscillations, and later increases further. This complex nonmonotonic behavior is due to penetration of slip from the nearby slowly slipping region. The creeping region concentrates stress at its edge, causing slip there and expanding itself. This process moves the stress concentration along the fault and results in time-dependent heterogeneity of shear stress within the nucleation zone. We find the corresponding fluctuations of slip velocity in all cases we have studied in the model with rheological transition. Note that variations in slip velocity are linked to variations of  $V\theta/L$ , the quantity important in the aftershock model of *Dieterich* [1994].

[33] Hence we find that earthquake nucleation in the two models proceeds differently, as demonstrated by slip velocity evolution of points within the nucleation zone. The differences are caused by spatial and temporal stress heterogeneity within the nucleation zone and result in significant consequences for aftershock rates (section 5).

#### 4. Dependence of Nucleation Processes and Sizes on Loading History

[34] As discussed in section 1, several simple analytical estimates  $h_{\text{nuc}} = \eta GL/(\bar{\sigma}F)$  for the nucleation size have been proposed. In particular,  $F = b$  was advocated by *Dieterich* [1992]. *Rubin and Ampuero* [2005] found that  $F = b$  is valid in a certain parameter regime,  $a/b \lesssim 0.37$ , while  $F = b/(b - a)^2$  holds for  $a/b \gtrsim 0.5$ . This is because, for  $a/b \gtrsim 0.5$  the condition  $V\theta/L \gg 1$  adopted by *Dieterich* [1992] breaks down in the middle of the nucleation zone under quasi-static tectonic loading. The *Dieterich* and *Rubin-Ampuero* estimates are quite different for the values of  $a$  close to  $b$ . *Rubin and Ampuero* [2005] mentioned that “the loading conditions play a role, and could potentially place nucleation in the regime  $V\theta/L \gg 1$  even for large  $a/b$ ”, citing a stress step and the associated instantaneous change in slip velocity as an example.

[35] We find that nucleation evolution and size are indeed strongly controlled by loading history. Our simulations of nucleation under slow tectonic loading result, for both models, in nucleation sizes consistent with the estimates of *Rubin and Ampuero* [2005] (section 3). However, other reasonable loading histories can make the nucleation size closer to the estimate of *Dieterich* [1992] even for the parameter range  $a/b \gtrsim 0.5$ . As an example, consider a nucleation process in the model with a weaker patch for a case conceptually similar to case 1 of section 3, but with  $L = 20 \mu\text{m}$ ,  $a/b = 0.94$ ,  $b = 0.016$ , and the weaker patch size of 200 m. If we use the model-dependent constants  $\eta$  from antiplane models ( $\eta = 2.5$  for *Dieterich*,  $\eta = 2/\pi$  for *Rubin and Ampuero*) multiplied by parameter  $Z = 4/3$  (Appendix A), the two estimates are 2.5 m and 162 m, respectively, with the *Rubin-Ampuero* estimate 65 times larger than that of *Dieterich*. We consider two cases: nucleation proceeding under slow tectonic loading (Figures 6a, 6c, and 6e) and nucleation that experiences, in addition to slow tectonic loading, a positive shear stress step 1 year before the original time to instability (Figures 6b, 6d, and 6f). We find that the perturbed case has a much smaller nucleation size than the unperturbed case, 5.5 m versus 53 m. The new time to instability is 0.014 year.

[36] The difference between the two scenarios can be explained by the evolution of  $V\theta/L$  in the nucleation zone, shown in Figures 6e and 6f. The unperturbed scenario is consistent with the study of *Rubin and Ampuero* [2005] and follows the evolution typical for values of  $a/b \gtrsim 0.5$ , with  $V\theta/L$  of order 1 in the middle of the nucleation zone for times close to instability (Figure 6e). In the perturbed case,  $V\theta/L$  becomes, after the shear stress step, much larger than 1 throughout the nucleation zone and  $V\theta/L$  reduces to one in the nucleation region only after tips of the rupture start to expand dynamically (inset in Figure 6f). Hence, because of the stress perturbation, the condition  $V\theta/L \gg 1$  becomes valid throughout the nucleation zone and stays valid until

the dynamic event, leading to a much smaller nucleation size more consistent with the estimate of *Dieterich* [1992].

[37] This example demonstrates how different loading conditions can change the nucleation process and, in particular, cause order-of-magnitude differences in nucleation sizes. In laboratory experiments, slow loading over tectonic timescales is not feasible, and much faster loading must be used, rapidly increasing  $V$  and potentially leading to  $V\theta/L \gg 1$  everywhere within the nucleation region even for  $a/b \gtrsim 0.5$ . This may explain why experiments of *Dieterich and Kilgore* [1996] were consistent with the results of *Dieterich* [1992], even though laboratory values of  $a/b$  often fall into the range  $a/b \gtrsim 0.5$ .

#### 5. Comparing Nucleation Processes by Their Response to Static Stress Changes and Resulting Aftershock Rates

[38] To understand whether the differences in slip velocity evolution during nucleation that we find for different models are practically important, we consider their effect on aftershock rates.

##### 5.1. Procedure for Determining Aftershock Rates

[39] Following *Dieterich* [1994], we consider a preexisting population of rate-and-state nucleation sites distributed in the volume of a prospective aftershock region (Figure 7a). Just prior to the time of the main shock, each site is at a different stage in the nucleation process so that the population of nucleation sites would result in a constant background earthquake rate if left unperturbed. The main shock perturbs the nucleation sites, causing the nucleation to proceed differently and resulting in a nonconstant rate, which can be called the aftershock rate. We consider the situation when the population experiences a static stress change in the form of a uniform positive shear stress step, except in section 6 where a case with a nonuniform stress step is studied.

[40] To compute the aftershock rate, we need to know how the rate-and-state nucleation at each site reacts to such change in stress. Let us denote by  $T$  the time from the application of the stress perturbation to the unperturbed failure time. We call  $T$  the original time to instability. Let us denote by  $f(T)$  the new time to instability, i.e., the changed time to instability due to the stress perturbation. To compute the aftershock rate, we only need to know  $f(T)$  for all  $T$  of interest. For monotonic  $f(T)$ , the aftershock rate  $R$  is given by [*Gomberg et al.*, 2000] (Appendix C)

$$\frac{R}{r} = \frac{dT}{df}. \quad (4)$$

For nonmonotonic  $f(T)$ , which arise in one of the models, the inverse dependence  $T(f)$  is multivalued, and equation (4) cannot be used. The approach we developed for that situation is described in Appendix C.

[41] For each nucleation example described in section 3, we find  $f(T)$  numerically by the following procedure. Each stage of a given nucleation process can be labeled by its time to instability  $T$  (Figure 7b). We select many values of  $T$  and, for each of them, we conduct a simulation in which we perturb the nucleation process by imposing a static stress

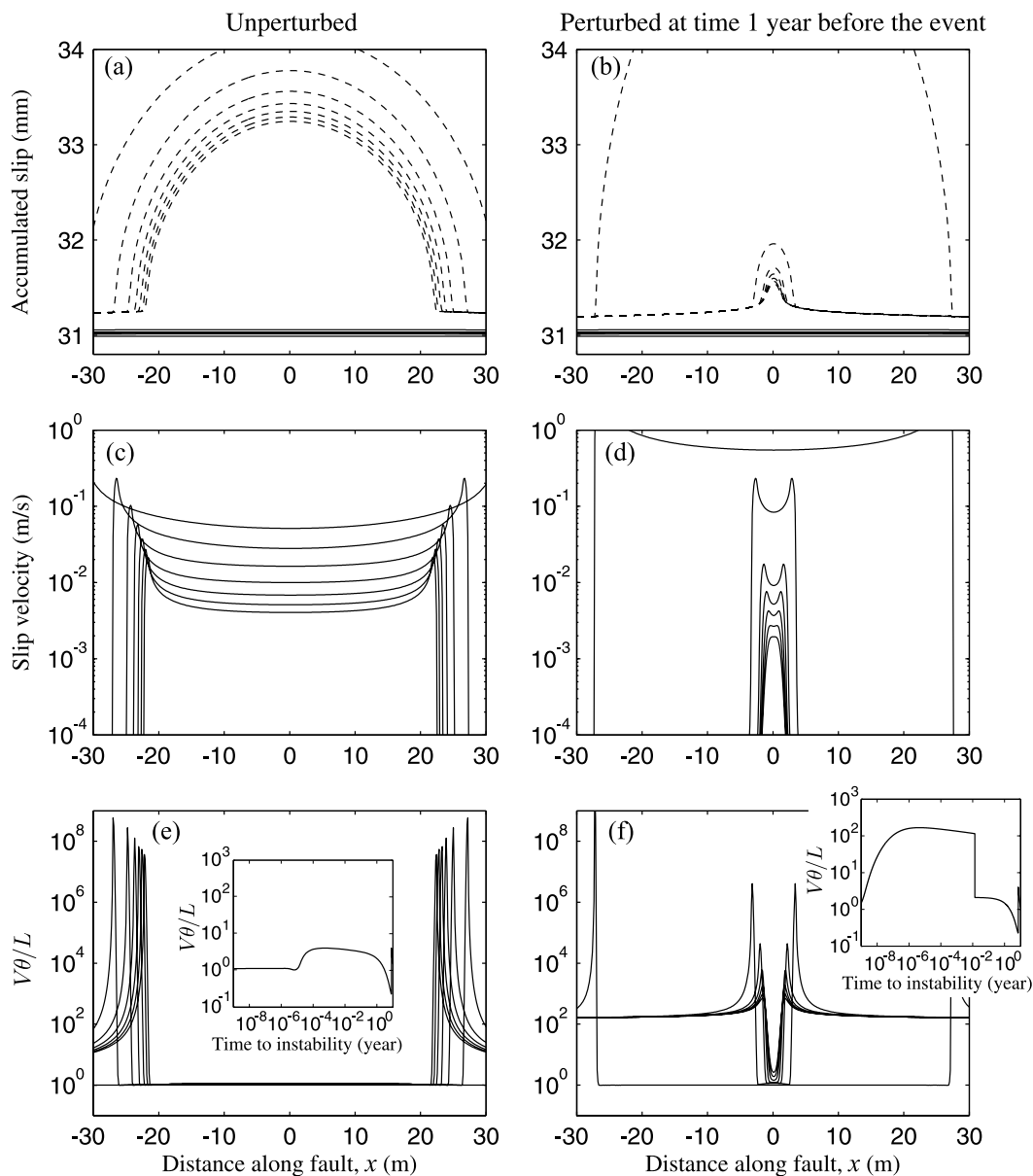


**Figure 6.** Dependence of nucleation processes on loading history. (a, c, and e) An unperturbed nucleation process in a model with a weaker patch,  $a = 0.015$ ,  $a/b = 0.94$ ,  $L = 20 \mu\text{m}$ , and the weaker patch size of 200 m. (b, d, and f) The same nucleation process but perturbed with  $\Delta\tau = 3.0 \text{ MPa}$  at 1 year before the original instability. The dashed lines in Figures 6a and 6b are plotted every 0.01 s starting with 0.05 s before our definition of the onset of instability. The solid lines in Figures 6c–6f correspond to the times of dashed lines from Figures 6a and 6b. The first five lines cluster, indicating the spatial extent of the nucleation zone. The insets show the evolution of  $V\theta/L$  at  $x = 0 \text{ m}$ . The nucleation sizes in these two cases differ by an order of magnitude.

step in the fault model at time  $T$  before the instability. In the simulation with the perturbation, the instability occurs at a different time, giving us the new time to instability  $f(T)$ . This numerically constructed  $f(T)$  is used to compute the aftershock rate.

[42] One of the important differences between our computation of aftershock rates and the model of *Dieterich* [1994] is that the original time to instability  $T$  in our model cannot be longer than the simulated interseismic period, whereas in the model of *Dieterich* [1994], the population of preexisting nucleation sites can include sites with any

original (or unperturbed) times to instability  $T$ . However, for any nonzero stressing rate  $\dot{\tau}$ , the assumption that nucleation processes can be arbitrarily long is not physically plausible. If  $\tau_{fail}$  is an upper bound of failure stress, then the nucleation site would have to fail within the time of the order of  $\tau_{fail}/\dot{\tau}$ . That consideration imposes a physical limit on how large the times to instability  $T$  can be in the preexisting population even in the model of *Dieterich* [1994], although, mathematically, analytical expression (B5) that relates the time to instability and slip velocity of each nucleation site can be used for any  $T$ .

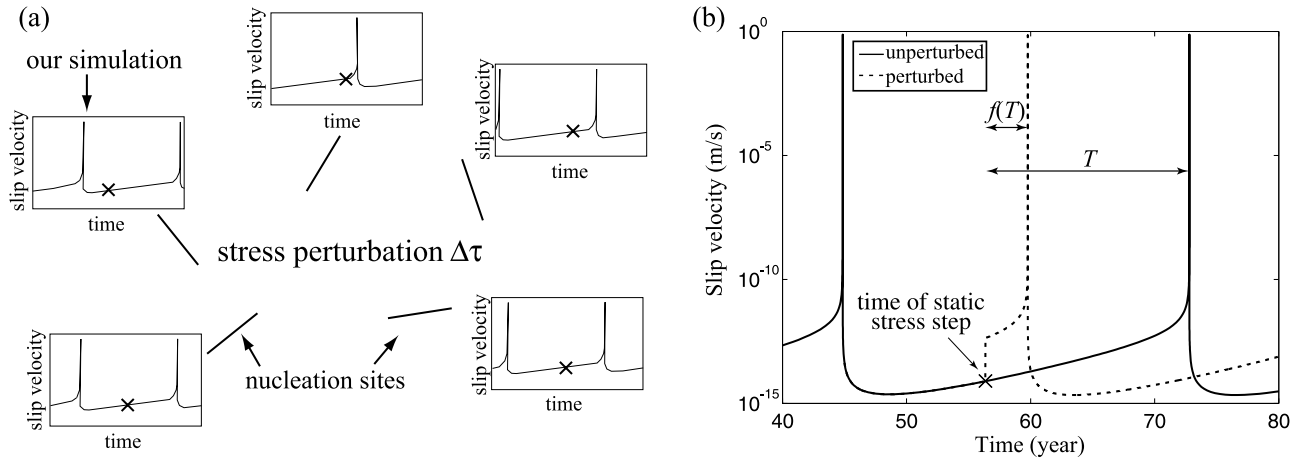


**Figure 7.** (a) A cartoon illustrating a population of nucleation sites just before a stress perturbation due to a main shock. Each nucleation site follows nucleation behavior simulated in a continuum fault model. At the time of the perturbation (shown by cross), nucleation sites are at different stages of the nucleation process, with the stages selected in such a way that the population would produce a constant (background) earthquake rate if left unperturbed. After stress step  $\Delta\tau$  due to the main shock, the population produces a nonconstant earthquake rate (aftershock rate). (b) Nucleation process of each site and its perturbation are illustrated using slip velocity at a representative point. The solid and dashed lines show the unperturbed and perturbed response, respectively. A static stress step is applied at the time indicated by cross.  $T$  and  $f(T)$  denote the original time to instability and the new time to instability, respectively. This example shows slip velocity at the middle of the nucleation zone for case 1. The model is perturbed at  $T = 16.4$  years before instability with a stress step  $\Delta\tau = 3.0$  MPa; the new time to instability is  $f(T) = 3.4$  years.

[43] Our method of computing aftershock rates can be used to find aftershock rates due to perturbations of any time-dependent nucleation process. In addition, this approach can be readily extended to dynamic perturbations and to more complex scenarios in terms of the initial nucleation population and spatial distribution of stress change. One such combined scenario, with spatially varying stress changes, is considered in section 6.

## 5.2. Aftershock Rates Based on Nucleation Processes at Weaker Patches: Overall Similarity to Spring-Slider Models, Effects of Heterogeneous Normal Stress

[44] Nucleation processes in the model with a weaker patch lead to response functions  $f(T)$  and aftershock rates shown as dotted lines in Figures 8a–8c and Figures 8d–8f, respectively. Each dot in Figures 8a–8c corresponds to a separate simulation. Note that a nucleation site with the new time to instability  $f$  will contribute to aftershock rates at the time  $f$  after the main shock, and that links the horizontal axes of Figures 8a–8c with those of Figures 8d–8f. For cases 1 and 2, the static stress step  $\Delta\tau = 3.0$  MPa is used; for case 3 of 10 times smaller  $a$ ,  $\Delta\tau = 0.30$  MPa is used, to have the same value of  $\Delta\tau/(a\bar{\sigma})$ . The analytical solutions of Dieterich [1994], computed from equations (B9) and (B5) of Appendix B, are shown for comparison as dashed lines. To compute the analytical solutions, we take the value of effective normal stress  $\bar{\sigma}$  corresponding to the average over the nucleation zone. The stressing rate  $\dot{\tau}$  is computed in our simulations by taking the time derivative of shear stress outside the nucleation zone (i.e., in the locked region). We find that  $\dot{\tau}$  is constant before and after the perturbation and equal to  $0.255$  MPa/a.

[45] The numerically computed response function  $f(T)$  and the corresponding aftershock rates nearly coincide with the analytical solution of Dieterich [1994] for case 1 (Figures 8a and 8d) of homogeneous  $\bar{\sigma}$  within the nucleation zone. A small deviation occurs only for times after the main shock smaller than  $10^{-7}$  years, as shown in the inset of Figure 8d. For heterogeneous  $\bar{\sigma}$  within the nucleation zone,  $f(T)$  and aftershock rates clearly deviate from the results of Dieterich [1994] (case 2, Figures 8b and 8e): The aftershock rates are higher right after the main shock, and there is a peak in the aftershock rates (Figure 8e). This is consistent with the differences in slip velocities for unperturbed nucleation processes discussed in section 3 (Figure 5). New times to instability smaller than  $10^{-2}$  years, for which the aftershock rates in case 2 are higher than in the model of Dieterich [1994] and higher than in case 1, correspond to original times to instability smaller than about  $10^0$  years, which is when unperturbed slip velocities of cases 1 and 2 develop more substantial differences (Figure 5b). Case 3 (Figures 8c and 8f) shows that decreasing the ratio  $a/b$ , while keeping the same value of  $\Delta\tau/(a\bar{\sigma})$ , the same value of  $(b - a)$ , and the same heterogeneity in normal stress, nearly eliminates the difference between the resulting aftershock rates and the analytical solution. For all three cases, the aftershock duration agrees with the prediction  $t_a = a\bar{\sigma}/\dot{\tau}$  of Dieterich [1994], as do the aftershock rates for times close to  $t_a$ . These results and their relation to the time evolution of slip velocity and the validity of the assumption  $V\theta/L \gg 1$  are further analyzed in sections 7 and 8.

[46] Aftershock rates exhibit a nearly constant value right after the stress step (Figures 8d–8f), which lasts for about 3 days in case 1. This plateau is consistent with the

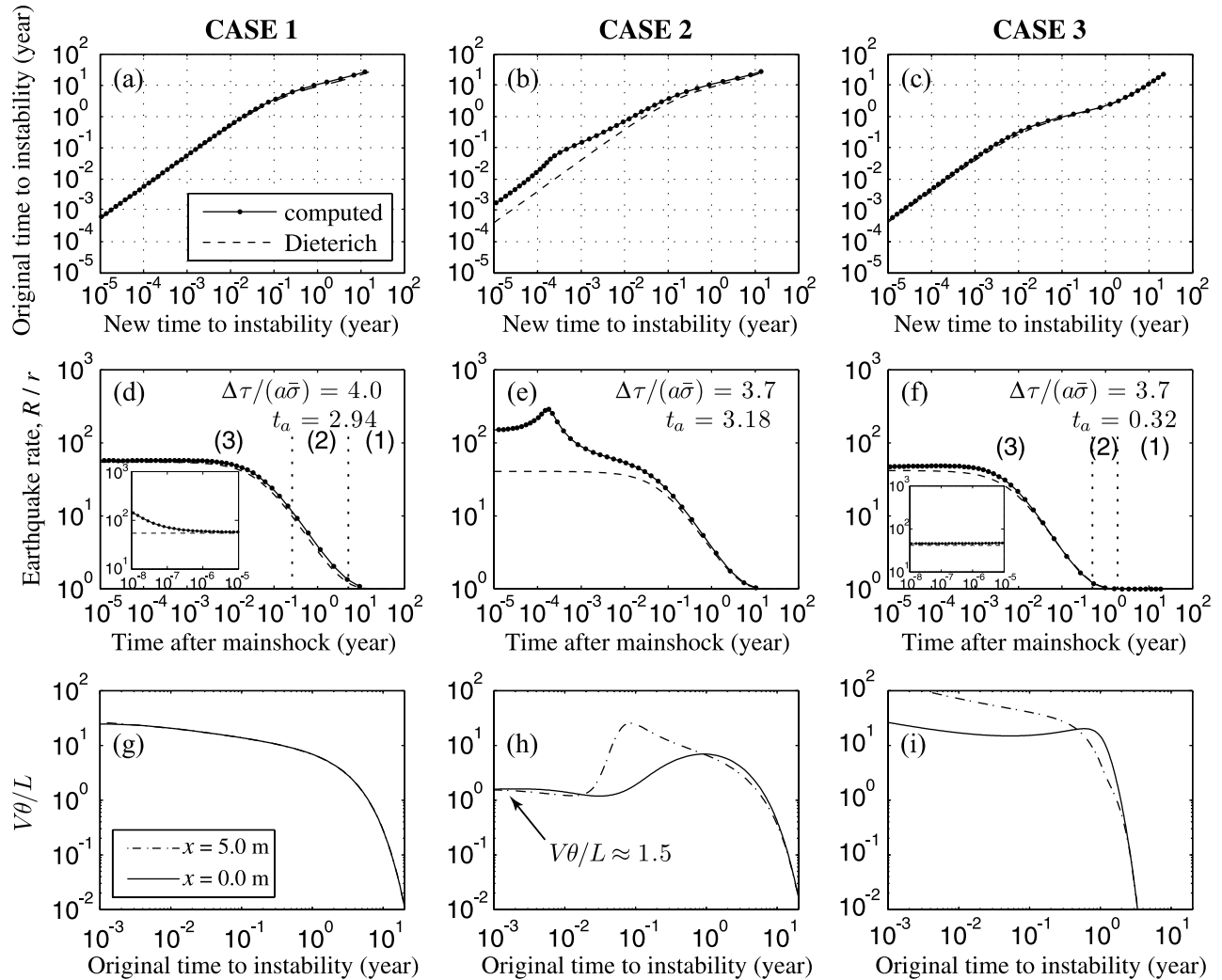


**Figure 8.** Response to static stress steps and the resulting aftershock rates for cases 1–3 of nucleation at a weaker patch. (a–c) Simulated response to stress steps (dotted solid lines) compared with the analytical results of *Dieterich* [1994] (dashed lines). In the text, the original time to instability is referred to as  $T$  and the new time to instability is referred to as  $f(T)$ . (d–f) Aftershock rates computed on the basis of Figures 8a–8c (dotted solid lines) and compared with *Dieterich*'s analytical result (dashed lines). The new time to instability in Figures 8a–8c corresponds to the time after the main shock in Figures 8d–8f. The normalized stress step  $\Delta\tau/(a\bar{\sigma})$  and the aftershock duration  $t_a = a\bar{\sigma}/\dot{\tau}$  for each case are indicated. (g–i) Evolution of  $V\theta/L$  before the dynamic event for unperturbed simulations at two locations inside the nucleation region.

prediction of spring-slider models. The plateau duration can be shortened by increasing the value of  $\Delta\tau/(a\bar{\sigma})$  (Appendix B). In case 1,  $\Delta\tau/(a\bar{\sigma}) = 4.0$  with  $\Delta\tau = 3.0$  MPa,  $\bar{\sigma} = 50$  MPa, and  $a = 0.01$ . Since  $\Delta\tau = 3.0$  MPa is already a high value for a static stress change, one can shorten the plateau duration only by using either smaller  $\bar{\sigma}$ , or smaller  $a$ , or both. That is why interpretations of aftershock observations using the model of *Dieterich* [1994] typically result in values of  $a\bar{\sigma}$  1 to 2 orders of magnitude smaller than the one we use in case 1 [*Gross and Kisslinger, 1997; Gross and Burgmann, 1998; Toda et al., 1998, 2005*]. Note that introduction of slight normal-stress heterogeneity in the nucleation region (case 2) results in higher aftershock rates after the main shock followed by a peak, and that behavior effectively shortens the duration of the plateau.

### 5.3. Aftershock Rates Based on Nucleation Processes at Rheological Transitions: Aftershock Peaks and Seismic Quiescence

[47] Figure 9 shows aftershock rates computed using nucleation processes from the model with rheological transition and compares them with the analytical rates computed on the basis of *Dieterich* [1994] (equation (B5)). Cases 4 and 5 are defined in section 2.2. In case 4, we apply shear stress step  $\Delta\tau$  such that  $\Delta\tau/(a\bar{\sigma}) = 0.4$ . In case 5, we use the same  $\Delta\tau$  that results in  $\Delta\tau/(a\bar{\sigma}) = 4.0$ . Case 6 is based on the nucleation process of case 4 but perturbed with a higher shear stress step corresponding to  $\Delta\tau/(a\bar{\sigma}) = 4.0$ . For the analytical solution of *Dieterich* [1994], we use  $\bar{\sigma} = 50$  MPa and  $\dot{\tau} = 0.087$  MPa/a; the value of the stressing rate is computed in our simulations by taking the time derivative of

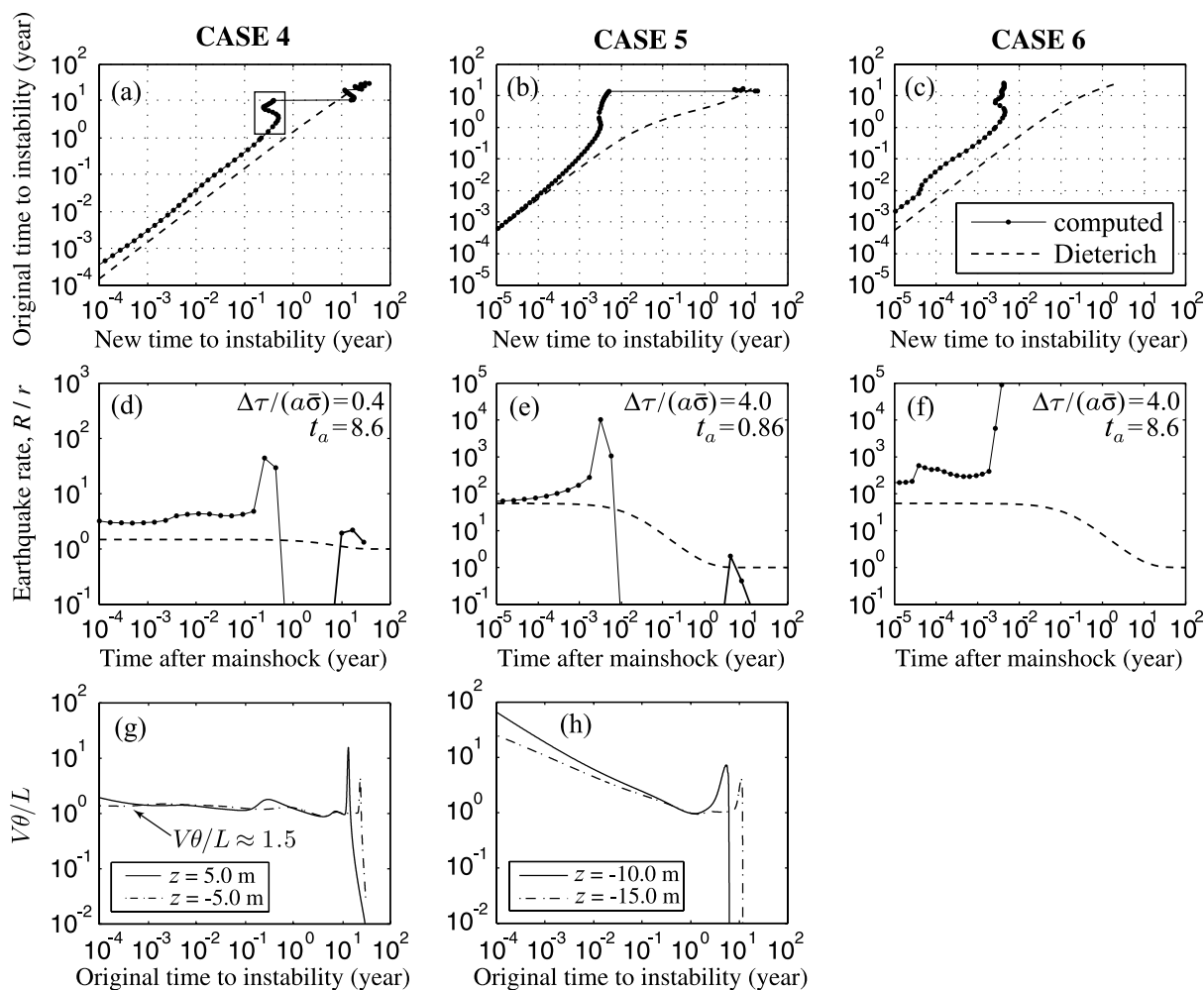


**Figure 9.** Response to static stress steps and the resulting aftershock rates for cases 4 and 5 of nucleation at rheological transitions. Lines have the same meaning as in Figure 8. Note that response  $f(T)$  to static stress changes and the resulting aftershock rates are nonmonotonic and qualitatively different from the analytical results of Dieterich [1994]. The box in Figure 9a indicates the part of  $f(T)$  shown in Figure C1.

shear stress within the locked region close to the nucleation zone (at  $z = 50$  m).

[48] In contrast to the behavior of nucleation processes due to weaker patches, nucleation processes due to rheological transitions give rise to complex nonmonotonic response  $f(T)$  (Figures 9a–9c). To understand the origin of the complexity, let us consider the effect of a static stress step applied to the nucleation process of case 4 at several different times. Figures 10a–10f give time histories of maximum slip velocity within a part of the velocity-weakening region,  $-32 \text{ m} \leq z \leq 50 \text{ m}$ , for both unperturbed and perturbed simulations. If the stress step is applied to the nucleation process when its original (unperturbed) time to instability  $T$  is 1 to 10 years, the triggered earthquake occurs in about 0.4 to 0.5 year (i.e.,  $f(T) = 0.4$  to 0.5 year), as illustrated in Figures 10a and 10b. That is why the aftershock rate for case 4 has a pronounced peak at about 0.4 to 0.5 year after the main shock (Figure 9d). However, stress perturbation at  $T = 11$  years results in a very different value of  $f(T) = 16$  years (Figure 10c), actually postponing the dynamic event. This is because the immediate consequence of the stress step is to induce more rapid slip but, for the perturbation at  $T =$

11 years, this more rapid slip fails to accelerate all the way to instability, relieving the elevated stress in the nucleation region aseismically and decreasing slip velocities throughout the nucleation zone (from the maximum of about  $10^{-11}$  m/s to  $10^{-14}$  m/s). That aseismic response postpones the next acceleration to dynamic instability and makes the new time to instability larger than the original time to instability.

[49] This behavior demonstrates how a positive shear stress step can delay the time to instability, inducing an aseismic slip transient instead of nucleating unstable slip sooner. The change in slip behavior is actually gradual for different  $T$ , with the size of the triggered earthquakes decreasing as the stress step is applied at values of  $T$  from 1 to 10 years, until, for  $T \gtrsim 10$  years, the stress step only causes transient acceleration of aseismic slip that fails to directly initiate a dynamic event. This is illustrated in Figures 10g–10i. For a stress step applied at  $T = 7.0$  years (Figure 10g), the triggered earthquake is of comparable size to events in the unperturbed simulation (Figure 3b) but the triggered event almost arrests halfway through, as evidenced by dense spacing of dashed lines, due to insufficient level of shear stress at locations from  $z = 60$  to  $z = 100$  m. For  $T =$

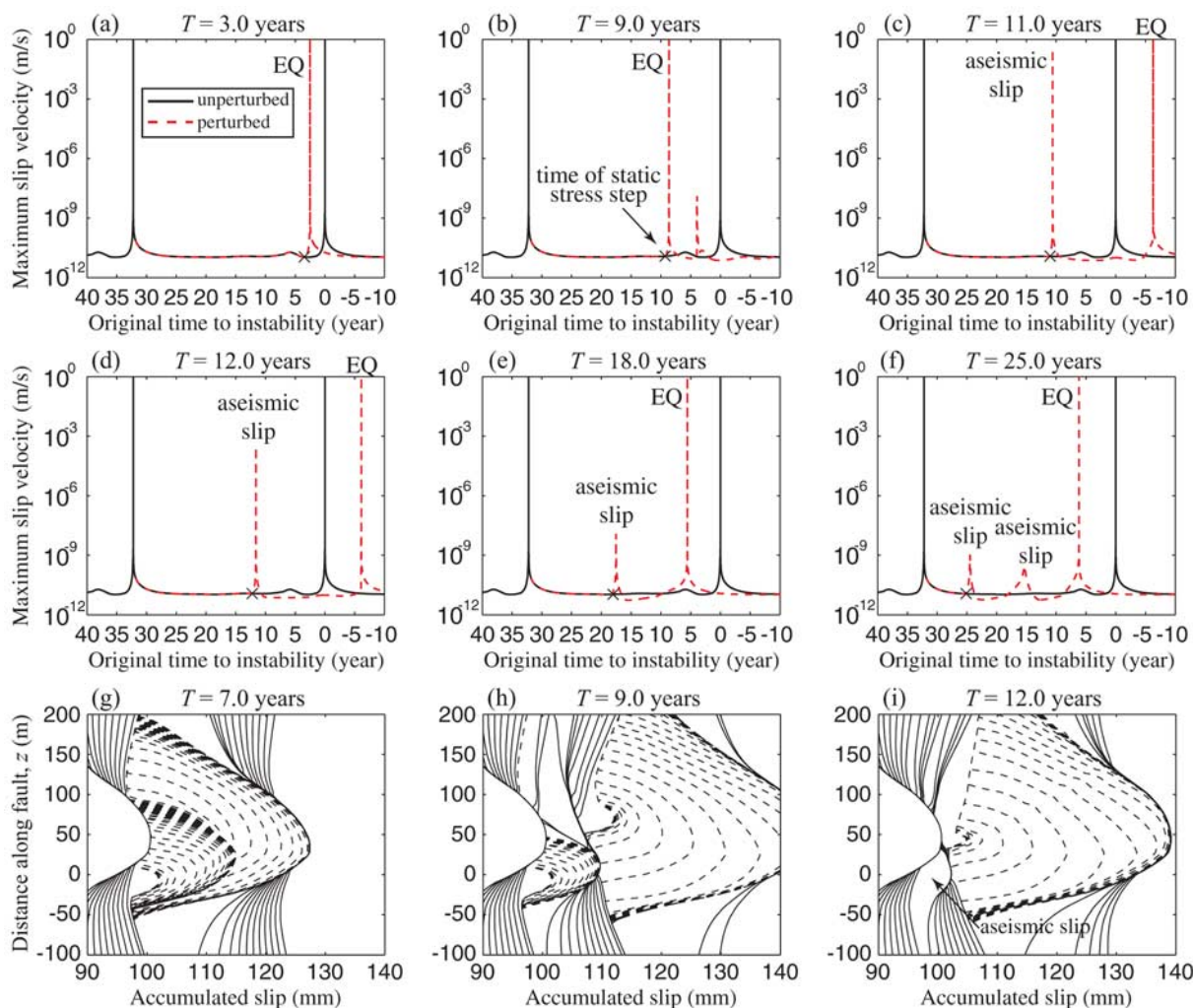


**Figure 10.** Response to static stress steps in the model with rheological transition (case 4). (a–f) Solid lines show the unperturbed evolution of maximum slip velocity within a part of the velocity-weakening region ( $-32 \text{ m} \leq z \leq 50 \text{ m}$ ) that contains the nucleation zone. Times of the stress perturbation are given on the top of each plot and marked by cross. Red dashed lines indicate the resulting perturbed behavior. (g–i) The effect of stress perturbations on the pattern of slip accumulation. The comparison between the plots is discussed in the text. Note that a positive shear stress step can delay the timing of the subsequent earthquake by inducing an aseismic transient (Figures 8c, 8d, and 8i).

9.0 years (Figure 10h), the triggered dynamic event is noticeably smaller than the unperturbed one; this is because shear stress further along the fault is not yet ready to support a larger event. Figure 10h also shows a larger event that occurs 20 years later. For  $T = 12.0$  years (Figure 10i), a stress step fails to induce dynamic instability and results in aseismic transient. The next seismic event occurs in 18 years (Figures 10d and 10i), which means that the stress step replaced the original time to instability of 12 years with the longer new time to instability of  $f(T) = 18$  years. For larger  $T$ , the triggered aseismic slip decreases in magnitude and area, relieving less of the accumulated stress and allowing the next dynamic event to initiate sooner, until the new time to instability is shorter than the original time to instability (Figure 10e). The smaller and smaller immediate impact of the stress step for larger values of  $T$  makes intuitive sense, since the model is farther from generating unstable slip. For stress steps at even larger values of  $T$ , the nucleation process

exhibits even more complex response, trying to accelerate twice before finally producing a dynamic event (Figure 10f).

[50] This response to static stress changes is more complex than the one found by *Perfettini et al.* [2003] in a similar model with rheological transition. *Perfettini et al.* [2003] concluded that the time advance of rate-and-state nucleation due to a static stress perturbation is similar to the one predicted by the Coulomb failure model for most of the earthquake cycle. This is similar to the conclusion we draw for some cases in the model with a weaker patch (section 8, scenario 1) but not for the model with the rheological transition. Simulations of *Perfettini et al.* [2003] used quasi-dynamic methodology that does not fully account for inertial effects as we do here, which may have diminished the slip response to abrupt stress changes. However, the main difference seems to be the selection of rate-and-state parameters and the resulting nucleation size. For the parameter selections in our models, nucleation sizes are

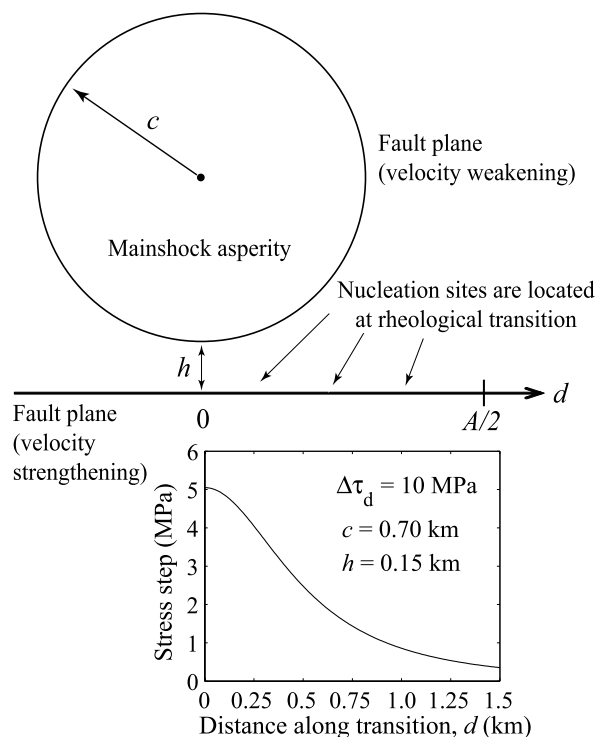


**Figure 11.** Model for estimating aftershock rates due to a population of nucleation sites located along a segment of rheological transition perturbed by a main shock asperity. Because of the distance from the asperity, the nucleation sites along the segment experience a nonuniform stress step. (top) Fault plane with a circular asperity of radius  $c$  and stress drop  $\Delta\tau_d$  that imposes a variable static stress step on the nucleation sites located along the transition shown by the horizontal axis. The variable  $d$  measures the distance along the transition. (bottom) Variation of static stress change with  $d$  for  $c = 0.70$  km,  $h = 0.15$  km, and  $\Delta\tau_d = 10$  MPa. The segment  $[-A/2, A/2]$  over which aftershock rates are sought is separated into subregions of approximately constant stress steps as discussed in the text.

several times smaller than the seismogenic region and nucleation occurs close to the rheological transition. Hence the expanding slow-slip region enters the zone of the eventual acceleration toward a dynamic event very early in the earthquake cycle, and the time- and space-dependent stress concentration at the tip of the slow-slip region constitutes a significant part of the nucleation zone. *Perfettini et al.*'s [2003] parameter choices led to much larger nucleation zone in the middle of the seismogenic zone, which formed after the slow-slip regions from both sides of the seismogenic region merged. That is likely why in the work of *Perfettini et al.* [2003], for most of the interseismic period, stress steps could only create an effect similar to Coulomb failure models, as described by scenario 1 of section 8.

[51] The aftershock rates computed on the basis of the complex nonmonotonic functions  $f(T)$  do not have power law decay and do not match the analytical solution of *Dieterich* [1994] (Figures 9d–9f), exhibiting a pronounced delayed peak followed by the period of very low or even zero aftershock rates (depending on whether one treats the

changes in  $f(T)$  discussed above as continuous or discontinuous during interpolations). Note that the smaller value of  $a/b$  in case 5 does not eliminate the significant differences between the numerically constructed aftershock rates and the analytical results of *Dieterich* [1994], as we have observed in the model with a weaker patch. In the model with rheological transition, the complex interplay of seismic and aseismic processes and the resulting complex aftershock response occur for all values of  $a/b$ , as the complexity is caused by the vicinity of rheological transition.

[52] The periods of zero or near-zero aftershock rates correspond to seismic quiescence. In case 4, all new times to instability are either larger than 11 years or smaller than 0.5 year. This means that there are no stages of the nucleation process that, when perturbed, result in new times to instability between 0.5 to 11 years. That is why there is quiescence of aftershocks in that time period (Figure 9d). Using spring-slider models, *Gomberg et al.* [2005] showed that quiescence at the end of the aftershock sequence can be explained by the absence of nucleation sites that are sufficiently far from instability. That is consistent with our results in case 6 (Figure 9f), where all available nucleation sites produce earthquakes in the first  $10^{-2}$  years after the stress perturbation, and there are no nucleation sites left to contribute to aftershock rates at later times. We emphasize that there is a different kind of quiescence in this model, one that originates not from the lack of nucleation sites but rather from the nonmonotonic response of nucleation processes to static stress changes.

#### 5.4. Dependence of Aftershock Rates on Constitutive Parameters $b$ and $L$

[53] Aftershock rates in the model of *Dieterich* [1994] do not depend on the rate-and-state parameter  $b$  and the characteristic slip  $L$ . In the continuum models presented here, aftershock rates show some dependence on parameters  $b$  and  $L$  for cases that exhibit deviations from *Dieterich*'s model. For nucleation processes due to weaker patches, aftershock rates depend on the ratio  $a/b$  and on the size of the weaker patch. Changing  $b$  while keeping  $a$  fixed would change the ratio  $a/b$ , while changing  $L$  would change the size of the nucleation zone and hence its relation to the size of the weaker region. For nucleation processes due to rheological transitions, the value of  $b$  affects the height of the delayed peak in aftershock rates, while decrease in  $L$  results in a shorter average time interval between earthquake nucleation at the same location, which can lead to more rapid initiation of seismic quiescence after a period of aftershocks.

#### 6. Aftershock Rates due to Nonuniform Stress Changes in the Model With Rheological Transition

[54] How would the delayed peaks in aftershock rates that we observe for the model with rheological transition superimpose for nonuniform stress changes due to the distance from the main shock? To answer this question, let us consider a population of nucleation sites uniformly distributed along the rheological transition and perturbed by shear stress change due to slip at a circular asperity (i.e., an area of large coseismic slip) located just above the transition (Figure 11). The population of nucleation sites along the

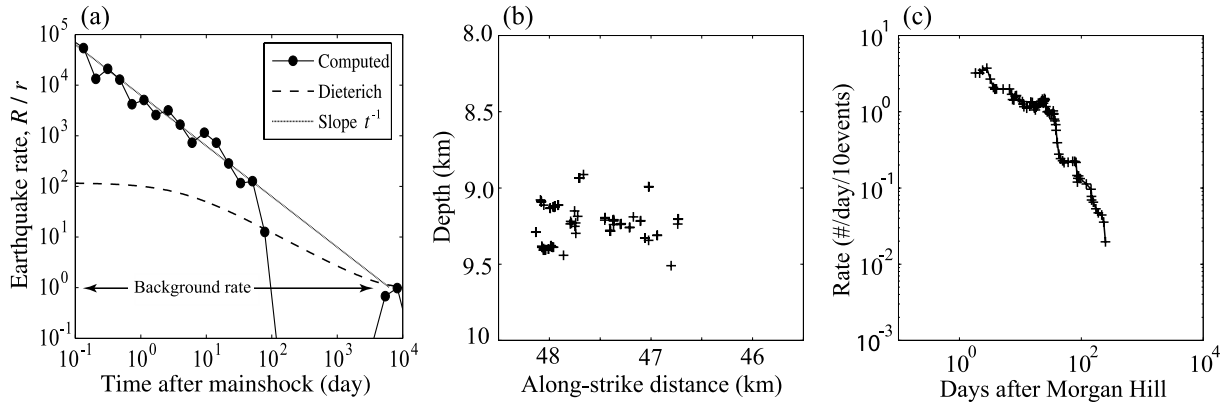


**Figure 12.** (a) Aftershock rates computed for the nonuniform static stress change and a population of nucleation sites located along the rheological transition (Figure 11). Dots represent the aftershock rates based on the model with rheological transition. The aftershock rate based on the work by *Dieterich* [1994], for the same friction and stress parameters, is shown by the dashed line. The slope of  $t^{-1}$  is plotted for reference. This model produces Omori's law in a limited time period followed by seismic quiescence. For the period of the power law decay of aftershocks, this model produces much higher aftershock rates than predicted by the model of *Dieterich* [1994]. Figures 12b and 12c are from *Tian and Rubin* [2005], courtesy of Y. Tian. A cluster of the 1984 Morgan Hill aftershocks occurred at a depth appropriate for rheological transition. (b) Cross-sectional view of one multiplet of aftershocks. (c) Observed seismicity rate versus time. The multiplet approximately followed Omori's law, but seismicity terminated about 1 year after the Morgan Hill earthquake. This behavior is qualitatively similar to that of the computed aftershock rates in Figure 12a.

transition experiences nonuniform stress step  $\Delta\tau$  that can be approximated by [*Dieterich*, 1994]

$$\Delta\tau = -\Delta\tau_{\text{drop}} \left[ \left( 1 - \frac{c^3}{[(c+h)^2+d^2]^{3/2}} \right)^{-1/2} - 1 \right], \quad (5)$$

where  $\Delta\tau_{\text{drop}}$  is the stress drop in the asperity,  $c$  is the asperity radius,  $h$  is the distance from the asperity edge to the transition, and  $d$  is the distance along the transition, with  $d = 0$  corresponding to the point directly below the hypocenter. In our example,  $\Delta\tau_{\text{drop}} = 10$  MPa,  $c = 0.70$  km, and  $h = 0.15$  km.

[55] We would like to determine aftershock rates due to a population of nucleation sites uniformly distributed along the segment  $[-A/2, A/2]$  of the transition. Each nucleation site is governed by the nucleation process of case 4. We divide the segment into subsegments  $A_i$ ,  $i = 1, 2, \dots$  such that the change of the stress step within each subsegment is 0.25 MPa. We assume that the stress step within each subsegment is constant and equal to the stress step at the center of the subsegment. The aftershock rate  $R_i/r$  for each subsegment  $A_i$  is determined using the approach developed in this work. The overall aftershock rate can then be obtained as the weighted sum:

$$\frac{R}{r} = \sum_i \frac{R_i}{r} \frac{A_i}{A}. \quad (6)$$

In our example,  $A/2 = 1.4$  km, which corresponds to selecting nucleation sites located approximately within one

asperity radius from the edge of the main shock. The computed aftershock rate shows a power law decay with time for about 1 year, and then quiescence (Figure 12a, dotted line). Evidence of turnoff of aftershock activity was found at the base of the seismogenic zone near the M6.2 1984 Morgan Hill earthquake [*Tian and Rubin*, 2005; Y. Tian, personal communication, 2005]. In that case, aftershocks followed Omori's law for several months and then disappeared (Figures 12b and 12c). This is qualitatively similar to our computed aftershock rate (Figure 12a). We emphasize that the correspondence is only qualitative; for example, we use a vastly simplified model of the main shock. Stress changes due to a realistic main shock may be quite heterogeneous locally, and direct quantitative comparison between models and observations would require a more detailed analysis.

[56] If the aftershock rate in our model were interpreted using the results of *Dieterich* [1994], the parameter  $a\bar{\sigma}$  would be significantly underestimated. To find the aftershock rate based on the work by *Dieterich* [1994], we use the weighted sum (6) with  $R_i/r$  given by the analytical formula (B5), which results in much smaller rates (Figure 12a, dashed line). To match the numerically computed aftershock rate, we need to use 10 times smaller  $a\bar{\sigma}$  in (B5) (and also 20 times smaller stressing rate  $\dot{\tau}$ , to match the slope). While this does not fully close the gap between the expected and observed values of  $a\bar{\sigma}$ , it is a step in the right direction. This example shows that application of spring-slider solutions to earthquakes that potentially have more complex nucleation processes, such as the ones occurring at rheological transitions, may lead to errors in estimating rate-and-state parameters.

[57] Similar superposition of aftershock peaks, leading to Omori's law in a limited time period, should arise in a

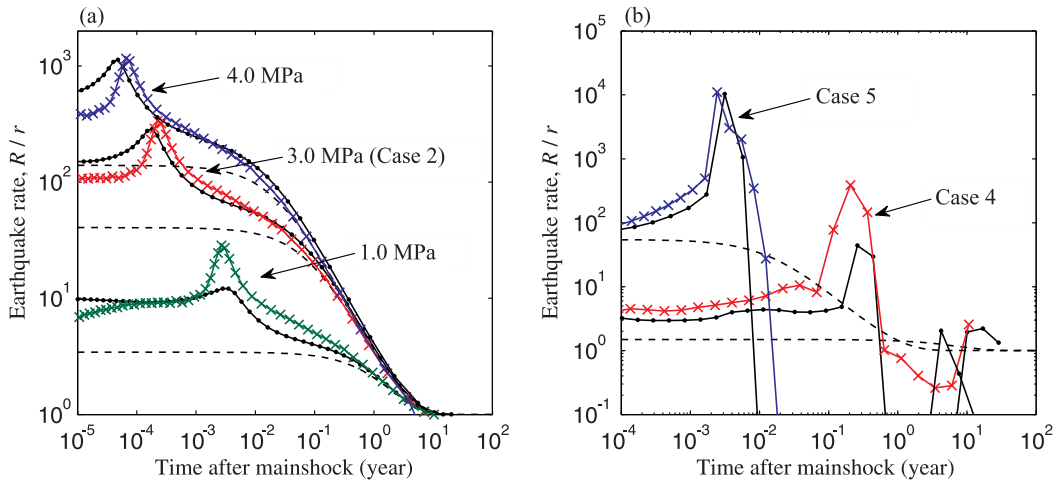


**Figure 13.** Comparison of the aftershock rates computed using simulations with stress perturbations (solid dotted lines), the semianalytical estimate based on equation (9) (lines with crosses), and analytical results of *Dieterich* [1994] (dashed lines). (a) Aftershock rates for case 2 and three different values of the stress step ( $\Delta\tau = 1.0, 3.0, 4.0$  MPa). (b) Aftershock rates for cases 4 and 5. In all cases, the semianalytical estimate qualitatively matches the main features of the computed aftershock rates. The analytical results of *Dieterich* [1994] are significantly different.

situation with a constant stress step  $\Delta\tau$  but applied to a population of nucleation sites with varying values of  $a\bar{\sigma}$ . For example, cases 4 and 5 have the same  $\Delta\tau$  but case 5 has ten times smaller  $a\bar{\sigma}$ , and, as a result, the aftershock rate peak is much larger in case 5 and occurs much earlier. These results suggest that it might be difficult to observe distinct peaks in aftershock rates on natural faults, because they would be obscured by nonuniform stress changes and/or variable values of  $a\bar{\sigma}$ . However, the model with rheological transition and the associated complex aftershock response may explain deviations from Omori's law in appropriately chosen subsets of aftershocks.

## 7. Link Between Aftershock Rates and Slip-Velocity History of Unperturbed Nucleation Processes

[58] The unperturbed slip velocity evolution in our models can be used to qualitatively capture the numerically computed aftershock rates. Let us denote slip velocity in a given nucleation process by  $V_g(T)$ . Each point of the nucleation zone in a continuum model has its own slip velocity evolution, so  $V_g(T)$  denotes a characteristic measure. For example, for the model with a weaker patch, we take slip velocity in the middle of the nucleation zone as  $V_g(T)$ . Let us assume that, after the perturbation,  $V_g\theta/L \gg 1$  in the nucleation zone for all subsequent times. Then the new time to instability can be found from the analysis of *Dieterich* [1994]:

$$f(T) = t_a \ln \left( \frac{\dot{\tau}}{H\bar{\sigma}V_g(T) \exp(\Delta\tau/(a\bar{\sigma}))} + 1 \right) \text{ for } \dot{\tau} \neq 0, \quad (7)$$

where  $H = -k/\bar{\sigma} + b/L$  and  $k$  is the effective stiffness of the nucleation zone. With each original time to instability  $T$ , we can associate slip velocity  $V_D(T)$  that the nucleation process

from *Dieterich* [1994] needs to have in order to nucleate an instability in time  $T$ :

$$T = t_a \ln \left( \frac{\dot{\tau}}{H\bar{\sigma}V_D} + 1 \right) \text{ for } \dot{\tau} \neq 0. \quad (8)$$

Combining (7) and (8), we can eliminate  $H$  and get

$$f(T) = t_a \ln \left( \frac{\exp\left(\frac{T}{t_a}\right) - 1}{\frac{V_g(T)}{V_D(T)} \exp\left(\frac{\Delta\tau}{a\bar{\sigma}}\right)} + 1 \right) \text{ for } \dot{\tau} \neq 0. \quad (9)$$

Similarly, one obtains

$$f(T) = \frac{T}{\frac{V_g(T)}{V_D(T)} \exp\left(\frac{\Delta\tau}{a\bar{\sigma}}\right)} \text{ for } \dot{\tau} = 0. \quad (10)$$

Equations (9)–(10) give an analytical approximation of  $f(T)$  that can be used to approximately compute aftershock rates. For  $V_g(T) = V_D(T)$ , we have a nucleation process that follows the model of *Dieterich* [1994], and in that case we recover (B3).

[59] Figure 13 shows comparison, for cases 2, 4, and 5, between the aftershock rates computed on the basis of numerous calculations with stress perturbations and the aftershock rates obtained on the basis of the approximate formula (9). We use the following unperturbed slip velocity histories as  $V_g(T)$ : at the center of the nucleation zone for case 2, at  $z = -5$  m for case 4, and at  $z = -20$  m for case 5. Since case 1 has the same friction parameters as cases 2 and 4, case 3 has the same friction parameters as case 5, and the aftershock rates for cases 1 and 3 generally agree very well with those based on the work by *Dieterich* [1994], we use the unperturbed slip velocity at the center of the nucleation

zone in cases 1 and 3 as  $V_D(T)$ . Note that cases 1 and 3 have about three times higher stressing rate (0.255 MPa/a) than cases 4 and 5 (0.087 MPa/a); hence we rerun the simulations for cases 1 and 3 with the correspondingly smaller value of the loading rate  $V_L$ .

[60] The semianalytical aftershock approximation qualitatively captures the computed aftershock rates for both models, for different stress steps and rate-and-state parameters (Figure 13). The overall agreement for the model with a weaker patch (Figure 13a) is better than for the model with rheological transition (Figure 13b). This is not surprising, as the semianalytical procedure is constructed assuming that the nucleation behavior after perturbation is well approximated by spring-slider models, and the model with a weaker patch compares much better with the results of spring-slider models than the model with rheological transitions (sections 3 and 5). Moreover, it is difficult to choose a representative slip velocity  $V_g$  for nucleation processes in the model with rheological transition: the nucleation zone is connected to the creeping region and hence its middle or extent is not easy to define, plus slip velocity within the nucleation region varies with distance in a nonsymmetric way. While slip velocity of most points gave qualitatively similar results, reproducing a pronounced peak and the following quiescence, the agreement in terms of timing and amplitude of those features was not as good for most points as shown in Figure 13b.

[61] The results suggest that (1) aftershock rates are linked to the unperturbed evolution of slip velocity and (2) once the differences in slip velocity history are accounted for, the spring-slider approximation can qualitatively match the aftershock rates, at least for the cases considered in this work. To use the semianalytical procedure predictively, i.e., without having the computed aftershock rates for comparison, one needs to establish an independent way of determining a representative slip velocity of a nucleation process. Whether this is possible to do for any nucleation process remains a question for future study.

## 8. Relation Between Aftershock Rates and the Validity of the State Evolution Assumption

[62] The aftershock model of *Dieterich* [1994] is based on nucleation processes governed by rate-and-state friction with the state evolution assumption  $V\theta/L \gg 1$ . Let us consider the validity of the assumption for nucleation processes in our models and how it relates to similarities and differences between our numerically computed aftershock rates and the results of *Dieterich* [1994].

### 8.1. Model With a Weaker Patch

[63] Figures 8g–8i show  $V\theta/L$  as a function of the original time to instability  $T$  for two representative points within the nucleation zone. In this model,  $V\theta/L$  varies for different locations within the nucleation zone but we find that a large part of the nucleation zone around its middle behaves similarly. In the following, we take the behavior of the middle point of the nucleation zone as being representative of the entire nucleation process. The temporal correspondence between  $V\theta/L$  in Figures 8g–8i and aftershock rates in Figures 8d–8f can be established by using the Figures 8a–8c: the horizontal axis in Figures 8g–8i corresponds to the vertical axis in Figures 8a–8c, and the

horizontal axis in Figures 8a–8c corresponds to the horizontal axis in Figures 8d–8f.

[64] The first important observation is that some of the nucleation sites considered in our aftershock rate calculations are characterized by  $V\theta/L < 1$  and even  $V\theta/L \ll 1$ , not  $V\theta/L \gg 1$  as assumed by *Dieterich* [1994]. As an example, consider case 3. Figure 8i shows that all nucleation sites with original times to instability larger than 2 years have  $V\theta/L < 1$ , and, for most of them,  $V\theta/L \ll 1$ . Nonetheless, Figure 8f shows that these rates match very well the model of *Dieterich* [1994], which assumes  $V\theta/L \gg 1$  at all times. This observation is consistent with the findings of *Gomberg et al.* [2000] for spring-slider models. To understand why the formulae of *Dieterich* [1994] still work in this situation, let us consider the aftershock behavior of nucleation zones that are far from failure. A shear stress step increases slip velocities by a factor of  $\exp[\Delta\tau/(a\bar{\sigma})]$ . Two scenarios can be distinguished in terms of the resulting aftershock rates.

[65] In scenario 1, slip velocities in the nucleation zone are small enough before the stress step so that the condition  $V\theta/L \ll 1$  holds both before and after the stress step. In this situation, the effect of stress step  $\Delta\tau$  on the nucleation site is approximately equivalent to the effect of gradual loading  $\dot{\tau}$  over time  $\Delta t = \Delta\tau/\dot{\tau}$  (Appendix D, section D1), with  $\Delta t$  independent of  $T$ . Hence we approximately have  $T - f(T) = \Delta\tau/\dot{\tau} = \text{constant}$  (or “constant clock advance”, in the terminology of *Gomberg et al.* [1998], who also identified this scenario) and  $R/r = dT/df = 1$ . This explains the origin of the aftershock rates equal to the background rate for case 3 (time period marked 1 in Figure 8f). Note that cases 1 and 2 (Figures 8d and 8e) do not have time periods during which the rates are equal to the background rate. For those cases, the nucleation processes at all times have such slip velocities that  $V\theta/L \gg 1$  after the stress step.

[66] In scenario 2, slip velocities in the nucleation zone are such that  $V\theta/L \ll 1$  before the stress step but  $V\theta/L \gg 1$  after the stress step and until the instability. The analysis of this scenario (Appendix D, section D2) predicts  $\{R\}/\{r\} = \{1\}/[1 - \exp(-f/t_a)]$ . For  $f \ll t_a$ , one has  $R/r = t_a/f$ , which shows a power law decay of the aftershock rate with the time  $f$  after the main shock. For  $f \gg t_a$ , one gets  $R/r = 1$  and the aftershock rate is equal to the background rate. The corresponding parts of the aftershock rates in Figures 8d and 8f are marked as time periods 2.

[67] For nucleation zones close to failure, which we define as those zones that have reached  $V\theta/L \gg 1$ , subsequent deviations of  $V\theta/L$  from the condition  $V\theta/L \gg 1$  create significant discrepancies in aftershock rates relative to the results of *Dieterich* [1994]. This is because such deviations reflect significant differences in slip velocity histories, and the importance of differences in slip velocity has already been shown (section 7). As an example, let us consider case 2 of heterogeneous effective normal stress within the nucleation zone. Figure 8e shows differences between the computed aftershock rates and the prediction (equation (B5)) of *Dieterich* [1994] for times shortly after the main shock. The nucleation zones that contribute to these differing aftershock rates have new times to instability  $f(T) < 10^{-2}$  years (Figure 8e) and original times to instability  $T < 1$  years (Figure 8b), with the corresponding values of  $V\theta/L$  in the middle of the nucleation zone that change from being much larger than 1 to the value of about 1.5.

A value of  $V\theta/L$  close to 1 violates the assumption  $V\theta/L \gg 1$  and causes the corresponding deviation in aftershock rates. Case 1 has a similar deviation in aftershock rates from the analytical solution (B5), for times after the main shock smaller than  $10^{-7}$  years (the inset in Figure 8d). That deviation is also related to values of  $V\theta/L$  being close to 1 in the middle of the nucleation zone during the very end of the nucleation process, for original times to instability that are outside of the time range shown in Figure 8g. In case 3, however, as the end of the unperturbed nucleation is approached, the condition  $V\theta/L \gg 1$  stays valid. As the result, the corresponding aftershock rates (Figure 8f) show close agreement with the model of *Dieterich* [1994]. Note that the behavior of  $V\theta/L$  for times close to instability is consistent with the study of *Rubin and Ampuero* [2005].

[68] The discrepancy between the computed aftershock rates and the ones based on the model of *Dieterich* [1994] right after the main shock can be estimated using appropriate assumptions in the spring-slider model (Appendix D, section D3). For cases 1 and 2 (Figures 8d and 8e), the simulated aftershock rates are 3.2 and 3.8 times larger than those predicted by the model of *Dieterich* [1994], while the two estimates derived in section D3 give factors of 2.7 and 3.5, matching the discrepancy relatively well.

## 8.2. Model With Rheological Transition

[69] Figures 9g and 9h illustrate the time evolution of  $V\theta/L$  for the unperturbed nucleation processes of cases 4 and 5 (case 6 uses the unperturbed process of case 4, but with a different stress step). Figures 9g and 9h show that condition  $V\theta/L \gg 1$  becomes valid and then violated relatively early in the earthquake cycle relative to the model with a weaker patch. Consistently, the aftershock rates are significantly different from the model of *Dieterich* [1994] (Figures 9d–9f). The variations in  $V\theta/L$  are due to penetration of slow slip from the nearby velocity-strengthening region. Note that the variations in  $V\theta/L$  make scenarios 1 and 2 of section 8.1 inapplicable to this model, as condition  $V\theta/L \ll 1$  holds for some points in the nucleation zone but not others, even for nucleation zones with large original times to instability; in particular,  $V\theta/L \gg 1$  at the tip of the propagating slow slip.

[70] Hence, in both models, similar behavior of  $V\theta/L$  causes similar effects in terms of aftershock rates. However, the history and spatial distribution of  $V\theta/L$  is different in the two models, resulting in qualitatively different aftershock behavior.

## 9. Conclusions

[71] Using two different fault models, we have simulated several plausible scenarios of spontaneous earthquake nucleation, investigated their response to static shear stress steps, and inferred the corresponding aftershock rates. Overall, nucleation processes at weaker patches are characterized by slip velocity evolution and aftershock rates similar to spring-slider models, although there are notable deviations. Nucleation processes at rheological transitions and the corresponding aftershock rates are significantly different.

[72] For both models, unperturbed slip velocity history of nucleation zones and the resulting aftershock rates are closely linked. In the model with a weaker patch, slip velocity in nucleation zones is very low for most of the interseismic

period, increasing approximately exponentially in response to the approximately constant stressing rate due to tectonic loading. This is similar to the behavior of spring-slider models and, in particular, to the analytical solution of *Dieterich* [1994]. Aftershock rates created by such far-from-failure nucleation zones closely follow the model of *Dieterich* [1994], despite the fact that the condition  $V\theta/L \gg 1$  is violated for such zones. Nucleation processes due to rheological transitions behave very differently in the interseismic period, due to penetration of slow slip from the nearby velocity-strengthening region and the associated time- and space-dependent variations in slip velocity and shear stress. As the result, neither  $V\theta/L \gg 1$  (as in the work by *Dieterich* [1994]) nor  $V\theta/L \ll 1$  (as in the model with a weaker patch) holds throughout the nucleation zone in the interseismic period. That is why the model with rheological transition results in qualitatively different aftershock rates. Another type of deviation of aftershock rates from the model of *Dieterich* [1994], evident in both models, occurs because of nucleation zones close to instability for the parameter range  $a/b \gtrsim 0.5$ , consistently with the analysis of *Rubin and Ampuero* [2005].

[73] Nucleation processes simulated with different loading histories can have nucleation sizes that differ by an order of magnitude and cannot be predicted by a single existing theoretical estimate. Nucleation sizes obtained with slow tectonic-like loading are consistent with the estimates of *Rubin and Ampuero* [2005]. For models with  $a/b \gtrsim 0.5$ , loading histories that involve positive shear stress steps can result in significantly smaller nucleation sizes, closer to the estimate of *Dieterich* [1992]. The behavior can be explained by the evolution of  $V\theta/L$  in the nucleation zone and implies that final nucleation stages of aftershocks and other triggered events may be different from those of events nucleating under slow tectonic loading. In particular, nucleation sizes of aftershocks may be significantly smaller.

[74] In the model with rheological transition, the response of nucleation processes to static stress changes is complex and nonmonotonic. For example, it is commonly assumed that favorable static stress changes should lead to earthquakes occurring sooner. We find that positive shear stress steps can *delay* the time to instability by inducing aseismic transients that relieve stress in the nucleation zone and postpone seismic slip. Recent observations have documented complex interactions of seismic and aseismic slip [*Schwartz and Rokosky*, 2007, and references therein], and our findings provide one more instance where such interactions may be important. If such behavior is common on natural faults, at least in certain environments, it may partially explain the cases of poor correlation between static stress changes and aftershock occurrence.

[75] Aftershock rates based on nucleation processes at rheological transitions exhibit pronounced peaks and seismic quiescence. This behavior is qualitatively different from that of nucleation processes due to weaker patches, from Omori's law, and from the results for spring-slider models. The behavior may explain faster decay of aftershock activity than that given by Omori's law with  $p = 1$  and delayed seismic quiescence reported in several observational studies [e.g., *Daniel et al.*, 2008, and references therein]. We have shown that superposition of such responses for spatially variable stress steps can result in Omori's law for a certain period of time followed by seismic quiescence, the behavior

supported by observations [Tian and Rubin, 2005]. If this computed aftershock rate were interpreted using the model of Dieterich [1994], the inferred values of  $a\bar{\sigma}$  would be an order of magnitude smaller than the ones used in the simulations. The result suggests that complexity of rate-and-state nucleation processes may be partially responsible for the discrepancy between the values of  $a\bar{\sigma}$  predicted on the basis of laboratory studies and inferred from aftershock observations based on the model of Dieterich [1994].

[76] The differences in nucleation processes and aftershock rates between the continuum and spring-slider models arise because of the presence of heterogeneity, either in normal stress or in friction properties. Hence the effect of fault heterogeneity on aftershock phenomena needs to be systematically examined. Note that the heterogeneity discussed here is the local one that affects nucleation processes at individual aftershock sites. Aftershock sequences are undoubtedly affected by another kind of heterogeneity, where different nucleation sites may have different friction properties, stress conditions, stressing rates etc, and hence follow different nucleation processes. Our approach can be used to study certain aspects of such “global” heterogeneity by simulating a number of nucleation processes with different desired friction properties and stress conditions, determining their responses to stress perturbations, and combining those responses into one aftershock rate.

[77] This study employs the aging form of the state-variable evolution equation. Other formulations have been proposed, as discussed in section 1. On the basis of preliminary results with the slip law, we predict that the main findings of this work would be qualitatively similar for other rate-and-state formulations, in the following sense. Nucleation in relatively homogeneous situations would still produce aftershock rates largely consistent with spring-slider models. Nucleation at rheological transitions would still exhibit peaks in aftershock activity followed by quiescence, since this response mostly comes from the slow slip penetrating from the nearby creeping region, the feature that would not qualitatively change for other rate-and-state formulations.

[78] Following earlier studies, we have assumed a population of nucleation sites that would result in a uniform background rate if left unperturbed. That assumption implies a certain distribution of initial conditions over the population at the time of the stress step and affects the resulting aftershock rates. But parts of aftershock sequences may result from nucleation sites created by coseismic processes such as bulk damage. Such nucleation sites would not have contributed to the background rate, and it may be possible to account for them by considering a different distribution of initial conditions over the population of nucleation sites in the developed approach.

[79] The qualitative differences we find between the presented models indicate that more studies are needed to understand which nucleation scenarios dominate on natural faults, how they respond to static stress changes, and whether spring-slider models can provide an adequate interpretation of that response. Natural faults may contain rate-and-state nucleation zones developing under a number of conditions, in which case the response of faults to static stress changes would combine a number of models of the kind considered in this work.

[80] Given that rate-and-state friction laws have been successfully used to explain a number of earthquake phenomena and that main shocks cause static stress changes, it is reasonable to assume that at least some, and perhaps most, of aftershocks are caused by static triggering of rate-and-state nucleation processes. At the same time, a number of studies have proposed models of aftershocks based entirely on other mechanisms, as discussed in section 1. The developed approach enables us to study the combined effect of two or more mechanisms on aftershock rates. For example, the response of rate-and-state nucleation to static stress changes can be combined in our models with the effect of increased loading rate due to aseismic processes, through prescribed variations in the loading rate. Such combined models would help investigate the relative importance of different aftershock-producing mechanisms.

## Appendix A: Elastodynamic Equations and Numerical Parameters

[81] The model with a weaker patch is based on the crustal plane model described by Lapusta [2001]. The only nonzero component of the displacement is in the along-strike direction  $x$  and it is averaged over the depth  $H_{\text{seismic}}$  of the fault. The elastodynamic equation for the depth-averaged displacement  $\bar{u}(x, y, t)$  is [Lehner et al., 1981; Lapusta, 2001]

$$Z^2 \frac{\partial^2 \bar{u}}{\partial x^2} + \frac{\partial^2 \bar{u}}{\partial y^2} + \frac{1}{H_{\text{eff}}^2} \left( \frac{1}{2} \text{sign}(y) V_L t - \bar{u} \right) = \frac{1}{c_s^2} \frac{\partial^2 \bar{u}}{\partial t^2}, \quad (\text{A1})$$

where  $H_{\text{eff}} = (\pi/4)H_{\text{seismic}}$ ,  $Z = 1/(1 - \nu)$ ,  $\nu$  is Poisson’s ratio, and  $c_s$  is the shear wave speed. We use  $H_{\text{seismic}} = 150$  m. The third term on the left-hand side of the equation represents coupling to regions that are steadily moving with slip velocity  $V_L$ . The crustal plane model of Lapusta [2001] incorporated a free surface and loading from a deeper region. In the model with a weaker patch, the seismogenic region is loaded by two regions and there is no free surface (Figure 1a). This leads to a factor of two in front of  $V_L$  in equation (A1). The effective shear wave speed in the direction of the strike is  $Zc_s = 4$  km/s for values  $\nu = 0.25$  and  $c_s = 3$  km/s used in this study. The along-strike slip is given by  $\delta(x, t) = \bar{u}(x, y = 0^+, t) - \bar{u}(x, y = 0^-, t)$ . Using the same notation as Lapusta et al. [2000] and Lapusta [2001], the typical numerical parameters are as follows. There are  $N_{\text{ele}} = 8192$  spatial elements along the simulated fault domain  $\lambda = 2000$  m. The ratio  $h^*/h = 50.1$  of the critical cell size  $h^*$  to the cell size  $h = 0.244$  m ensures well-resolved simulations [Lapusta et al., 2000]. Time  $t$  is discretized into variable time steps, with the minimum value of  $0.25 h/c_s = 15 \mu\text{s}$  and the maximum value of 0.2 year. In the mode-dependent convolution truncation,  $T_w(1) = \lambda/c_s$  and  $q_w = 4$ .

[82] The elastodynamic equations and simulation methodology for the model with rheological transition are the same as by Lapusta et al. [2000]. The simulated fault domain  $\lambda = 1200$  m is composed of the 600-m region where friction is applied, and the 600-m loading region of the prescribed slip rate. The model of Lapusta et al. [2000] also included a mirror fault image to simulate the effects of a free surface, but the model in this work does not contain a free surface.  $\lambda$  is discretized into  $N_{\text{ele}} = 4096$  equal spatial

elements, each with the size  $h = 0.29$  m, so that  $h^*/h = 32.2$ . For time discretization and convolution computation, we use the same parameters as in the model with a weaker patch.

### Appendix B: Model of Aftershocks by Dieterich [1994]

[83] In the study of Dieterich [1994], each nucleation site was assumed to proceed through the slip stress history that would occur in a spring-slider system with the aging form (equations (1) and (2)) of rate-and-state friction. In that model, frictional sliding occurs on the block-substrate interface, which serves as the model of a fault. The spring of stiffness  $k$  provides elastic interactions. The governing equation for slip  $\delta(t)$  is given by

$$\tau^o + \dot{\tau}t - k\delta = \bar{\sigma} \left[ \mu_0 + a \ln\left(\frac{V}{V_0}\right) + b \ln\left(\frac{V_0 \theta}{L}\right) \right], \quad (\text{B1})$$

where the left-hand side gives shear stress on the interface with inertial effects ignored, the right-hand side gives the rate-and-state frictional resistance of the interface,  $\tau^o$  is shear stress that would act on the interface if it were constrained against slip and  $\dot{\tau}$  is the stressing rate applied directly to the interface. The rate-and-state formulation is simplified by assuming that, during nucleation, slip accelerates fast enough for the state variable to be significantly larger than its steady state value, so that  $V\theta/L \gg 1$ . The assumption  $V\theta/L \gg 1$  leads to the following state evolution:

$$\frac{d\theta}{d\delta} = -\frac{\theta}{L} \text{ and thus } \theta = \theta_{\text{ref}} \exp\left(-\frac{\delta - \delta_{\text{ref}}}{L}\right), \quad (\text{B2})$$

where  $\delta_{\text{ref}}$  and  $\theta_{\text{ref}}$  are reference values.

[84] In this model, the time to instability  $T$  can be obtained analytically [Dieterich, 1994]:

$$T = \frac{a\bar{\sigma}}{\dot{\tau}} \ln\left(\frac{\dot{\tau}}{H\bar{\sigma}V} + 1\right), \quad \text{for } \dot{\tau} \neq 0 \quad (\text{B3})$$

$$T = \frac{a}{HV}, \quad \text{for } \dot{\tau} = 0, \quad (\text{B4})$$

where  $H = -k/\bar{\sigma} + b/L$ . A population of nucleation sites that results in a uniform background rate  $r$  is created by assigning the appropriate distribution of initial slip velocity  $V$  to the population. A positive shear stress step  $\Delta\tau$  increases the initial slip velocity by a factor of  $\exp[\Delta\tau/(a\bar{\sigma})]$ , changing the time to instability for each nucleation site and resulting in a different earthquake rate  $R$  (aftershock rate) given by

$$\frac{R}{r} = \frac{1}{[\exp(-\Delta\tau/(a\bar{\sigma})) - 1] \exp(-t/t_a) + 1}, \quad (\text{B5})$$

where  $t_a = a\bar{\sigma}/\dot{\tau}$  and constant stressing rate  $\dot{\tau}$  is assumed before and after the stress step. Dieterich [1994] also considered scenarios with variable stress steps and stressing rates.

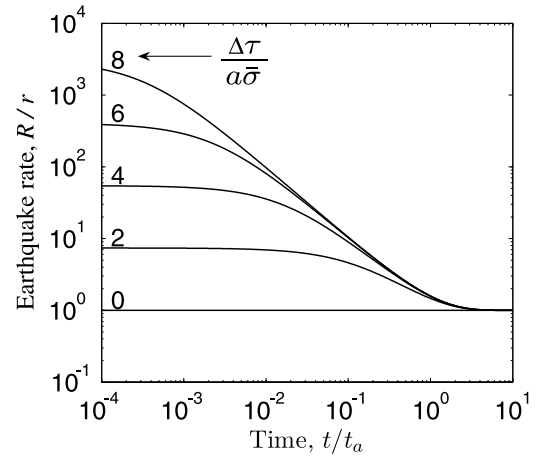


**Figure B1.** Aftershock rates for the analytical solution of Dieterich [1994] given by equation (B5). The aftershock rate  $R$  is normalized by the background rate  $r$  and the time  $t$  after the main shock is normalized by the aftershock duration  $t_a$ . Each curve is computed for a normalized stress step,  $\Delta\tau/(a\bar{\sigma})$ , with the indicated value. Adapted from Figure 2 of Dieterich [1994].

[85] From expression (B5), this model has two parameters:  $\Delta\tau/(a\bar{\sigma})$  and  $t_a = a\bar{\sigma}/\dot{\tau}$ . Figure B1 illustrates the resulting aftershock rates and shows that  $t_a$  is related to the aftershock duration, since the earthquake rate becomes close to the background rate for  $t \geq t_a$ . From (B5),  $R/r = 1$  for  $t \gg t_a$ . For  $t \ll t_a$ ,  $\exp(-t/t_a) \approx (1 - t/t_a)$  and from (B5),

$$R = \frac{K}{(c + t)^p}, \quad p = 1 \quad (\text{B6})$$

$$K = \frac{rt_a}{1 - \exp(-\Delta\tau/(a\bar{\sigma}))}, \quad c = \frac{t_a}{\exp(\Delta\tau/(a\bar{\sigma})) - 1}. \quad (\text{B7})$$

Hence the model of Dieterich [1994] interprets parameters  $K$  and  $c$  of Omori's law, which were originally introduced as empirical constants. The time interval in which the aftershock rates in this model follow the power law decay of aftershocks depends on the values of  $\Delta\tau/(a\bar{\sigma})$  and  $t_a$ . For times right after the instability, we have  $\exp(-t/t_a) \approx 1$  and  $R/r = \exp[\Delta\tau/(a\bar{\sigma})]$ . This "plateau" or constant aftershock rate right after the main shock is shorter for larger values of  $\Delta\tau/a\bar{\sigma}$  (Figure B1).

[86] Since static stress changes  $\Delta\tau$  due to earthquakes are relatively well constrained, aftershock observations can be used to constrain the product  $a\bar{\sigma}$ . For the model to be consistent with observations,  $a\bar{\sigma}$  has to be of the order of 0.01–0.1 MPa [Toda et al., 1998; Belardinelli et al., 1999]. Larger values of  $a\bar{\sigma}$ , of order 1 MPa, are predicted by laboratory values of  $a$  (of order 0.01) and  $\bar{\sigma}$  comparable to overburden minus hydrostatic pore pressure at typical seismogenic depths (of order 100 MPa). If aftershock production is dominated by static stress triggering of pre-existing nucleation sites, then, at least on parts of faults where aftershocks nucleate, either the direct effect coefficient  $a$  is much smaller than in the laboratory, or effective normal stress  $\bar{\sigma}$  is abnormally low.

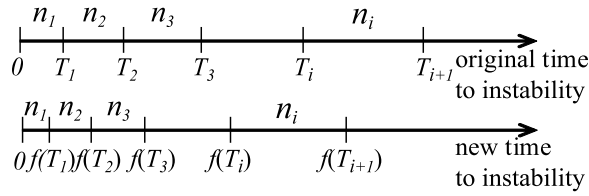


**Figure C1.** Schematics showing how the time to instability for each nucleation site in the population changes due to a stress step for a monotonic function  $f(T)$ . The top arrow represents the (original) time to instability  $T_i$  for the  $(\sum_{k=1}^i n_k)$ th nucleation site in the absence of perturbation, where  $n_i$  is the number of earthquakes between  $T_{i-1}$  and  $T_i$ . The bottom arrow shows the (new) time to instability  $f(T_i)$  after the static stress step at time zero. The time to instability of each nucleation site changes, resulting in a different earthquake rate (aftershock rate).

[87] The dependence  $f(T)$  for the model of *Dieterich* [1994] can be derived using the time-to-instability expression (B4). With  $V \exp[\Delta\tau/(a\bar{\sigma})]$  in (B3) instead of  $V$ , we obtain

$$f = \frac{a\bar{\sigma}}{\dot{\tau}} \ln \left( \frac{\dot{\tau}}{H\bar{\sigma}V \exp(\Delta\tau/(a\bar{\sigma}))} + 1 \right). \quad (\text{B8})$$

Solving (B3) for  $\dot{\tau}/(H\bar{\sigma}V)$  and substituting this quantity into (B8), we find

$$f(T) = t_a \ln \left( \frac{\exp(T/t_a) - 1}{\exp(\Delta\tau/(a\bar{\sigma}))} + 1 \right), \quad (\text{B9})$$

where  $t_a = a\bar{\sigma}/\dot{\tau}$ . We use (B9) for comparison with our simulations.

## Appendix C: Aftershock Rate Calculations

### C1. Monotonic Response $f(T)$

[88] We compute aftershock rates based on function  $f(T)$  that gives the perturbed (or new) time to instability for a nucleation site with the unperturbed (or original) time to instability  $T$  (Figure 7b). Without the perturbation, the population of rate-and-state nucleation sites should produce earthquakes at a constant background rate  $r$ . Hence, if one considers discrete time intervals  $[T_{i-1}, T_i]$ ,  $T_0 = 0$ ,  $T_i \geq T_{i-1}$ ,  $i = 1, 2, 3, \dots$ , with each of the intervals containing  $n_i$  earthquakes (Figure C1), then  $T_i$  and  $n_i$  have to satisfy the following relations:

$$r = \frac{n_1}{T_1 - T_0} = \frac{n_2}{T_2 - T_1} = \dots = \frac{n_i}{T_i - T_{i-1}}. \quad (\text{C1})$$

If  $f(T)$  is monotonic, then  $n_i$  earthquakes that would have occurred in the time interval  $[T_{i-1}, T_i]$  before the perturbation occur in the time interval  $[f(T_{i-1}), f(T_i)]$  after the perturbation (Figure C1). Hence the new earthquake rate  $R$  in each time interval is given by  $R[f(T_{i-1}), f(T_i)] =$

$n_i/(f(T_i) - f(T_{i-1}))$ . Using (C1), we obtain the normalized aftershock rate  $R/r$  as

$$\frac{R[f(T_{i-1}), f(T_i)]}{r} = \frac{T_i - T_{i-1}}{f(T_i) - f(T_{i-1})}, \quad (\text{C2})$$

or, in the limit of infinitely small lengths  $(T_i - T_{i-1})$  of the time bins,

$$R/r = dT/df. \quad (\text{C3})$$

This procedure for computing the aftershock rate  $R/r$  for monotonic  $f(T)$  is analogous to the one of *Gomberg et al.* [2000]. Using equation (C3) with  $f(T)$  for the model of *Dieterich* [1994], given by (B9), provides an alternative way of deriving the analytical aftershock rates (B5).

### C2. Nonmonotonic Response $f(T)$

[89] Expression (C3) is valid only for monotonic functions  $f(T)$ , as it requires the existence of the inverse function  $T(f)$ . For nucleation processes at rheological transition, however, functions  $f(T)$  turn out to be non-monotonic for all cases we have considered. As an illustration, consider  $f(T)$  given in Figure C2. Aftershocks occurring in the time interval  $\Delta f$  come from nucleation sites that, without perturbation, would have produced earthquakes in three time intervals  $\Delta T_1$ ,  $\Delta T_2$ , and  $\Delta T_3$ . Thus, the aftershock rate in the time interval  $\Delta f$  in Figure C2 is given by

$$\frac{R}{r} = \left| \frac{\Delta T_1}{\Delta f} \right| + \left| \frac{\Delta T_2}{\Delta f} \right| + \left| \frac{\Delta T_3}{\Delta f} \right|. \quad (\text{C4})$$

[90] To compute aftershock rates for a nonmonotonic  $f(T)$ , we create time bins  $\Delta f$  equally spaced on the

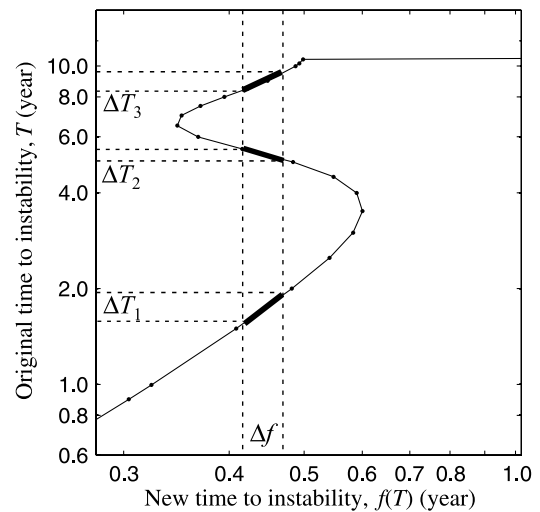


**Figure C2.** An example of a nonmonotonic  $f(T)$ . This is an actual response observed in the model with rheological transition for case 4. The data shown here are taken from the rectangle in Figure 9a. The bold lines on the curve represent three time intervals  $\Delta T_1$ ,  $\Delta T_2$  and  $\Delta T_3$  that contribute to the aftershock rate in the interval  $\Delta f$ .

logarithmic scale. That is, we choose  $\Delta f_j = f_j - f_{j-1}$ , where  $\log(f_j) - \log(f_{j-1}) = \log(f_j/f_{j-1})$  is the same for all  $j$ . For each  $f_j$ , we find the corresponding values of  $T_j$  by linearly interpolating discretely specified correspondence  $T(f)$ . Each  $f_j$  may have more than one corresponding  $T_j$ , or equivalently, each interval  $\Delta f_j$  may have several corresponding intervals  $\Delta T_{j(k)}$ . The aftershock rates can be obtained by adding the contribution of each  $\Delta T_{j(k)}$  to the corresponding time bin  $\Delta f_j$ :

$$\frac{R}{r} \Big|_{\Delta f_j} = \sum_k \left| \frac{\Delta T_{j(k)}}{\Delta f_j} \right|. \quad (\text{C5})$$

This procedure allows us to compute aftershock rates for complicated nonmonotonic responses that we observe in the model with rheological transition.

## Appendix D: Aftershock Rates for Simplified Scenarios

[91] In the model of *Dieterich* [1994] (Appendix B), it is assumed that zones nucleating earthquakes always satisfy the condition  $V\theta/L \gg 1$ . In our simulations, nucleation zones that contribute to aftershock response do not always satisfy that condition (section 8). To understand the contribution of such zones to aftershock rates, we consider here several simplified scenarios motivated by our simulations, using the spring-slider model (B1).

### D1. Scenario 1: Nucleation Zones With $V\theta/L \ll 1$ Before and After the Perturbation

[92] Our simulations in the model with a weaker patch show that, for much of the interseismic period,  $V\theta/L \ll 1$  in the nucleation zone because of the near-zero slip velocities  $V$ . Let us consider such a nucleation site at a time  $t_{\text{ref}}$ , approximating it as a spring-slider system with slip  $\delta_{\text{ref}}$ , slip velocity  $V_{\text{ref}}$ , state variable  $\theta_{\text{ref}}$ , and loading stress  $\tau_{\text{ref}}^o$  so that

$$\tau_{\text{ref}}^o - k\delta_{\text{ref}} = \bar{\sigma}[\mu_0 + a \ln(V_{\text{ref}}/V_0) + b \ln(V_0\theta_{\text{ref}}/L)]. \quad (\text{D1})$$

Since  $V\theta/L \ll 1$ , the evolution of state variable can be simplified to  $\theta(t) = \theta_{\text{ref}} + (t - t_{\text{ref}})$ , and near-zero slip velocities  $V$  imply that we can approximately write  $\delta(t) = \delta_{\text{ref}}$ . The governing equation (B1) becomes

$$\begin{aligned} \tau_{\text{ref}}^o - k\delta_{\text{ref}} + \dot{\tau}(t - t_{\text{ref}}) \\ = \bar{\sigma} \left[ \mu_0 + a \ln\left(\frac{V}{V_0}\right) + b \ln\left(\frac{V_0(\theta_{\text{ref}} + (t - t_{\text{ref}}))}{L}\right) \right]. \end{aligned} \quad (\text{D2})$$

From equations (D1) and (D2), we find the following time evolution of slip velocity:

$$V(t) = V_{\text{ref}} \exp \left[ \frac{t - t_{\text{ref}}}{t_a} - \frac{b}{a} \ln \left( 1 + \frac{t - t_{\text{ref}}}{\theta_{\text{ref}}} \right) \right]. \quad (\text{D3})$$

In (D3), slip velocity increases approximately exponentially with time, which is the same functional dependence as in the

model of *Dieterich* [1994] for times far from instability. The behavior is similar because, for times far from instability, slip velocities and hence slip accumulation are very small, the state variable evolves slowly, and the assumption regarding  $V\theta/L$  does not make much difference.

[93] After positive static stress step  $\Delta\tau$  at time  $t > t_{\text{ref}}$ , slip velocity  $V$  abruptly increases to  $V \exp[\Delta\tau/(a\bar{\sigma})]$ . In the nucleation process without perturbation, such larger slip velocity would be achieved only after time  $\Delta t$  such that  $V(t) \exp[\Delta\tau/(a\bar{\sigma})] = V(t + \Delta t)$ . Using equation (D3) (which is applicable both before and after the perturbation, due to the assumption that  $V\theta/L \ll 1$  holds for both stages), with the logarithmic term under the exponential ignored in comparison with the linear term, this leads to  $\Delta t = \Delta\tau/\dot{\tau}$ , consistently with the time advance for Coulomb-like behavior [*Gomberg et al.*, 2000; *Perfettini et al.*, 2003]. In the same time period, the state variable would change as well but if we ignore that (since the change in state variable is linear with time while the change of slip velocity is exponential), then the effect of the stress step is to essentially advance the nucleation process by a constant time  $\Delta\tau/\dot{\tau}$ . Using  $R/r = dT/df$  with  $f(T) = T - \Delta\tau/\dot{\tau}$ , we find  $R/r = 1$ . Hence nucleation sites considered in this scenario, taken by themselves, result in the aftershock rate equal to the background rate. Their time to instability is advanced, but by the same amount, so there is no pile up of the resulting earthquakes.

### D2. Scenario 2: Nucleation Zones With $V\theta/L \ll 1$ Before the Perturbation but $V\theta/L \gg 1$ After the Perturbation

[94] In this scenario, equations (D1)–(D3) continue to be valid. Let  $T_{\text{ref}}$  be the time to instability corresponding to time  $t_{\text{ref}}$  and  $T$  be the time to instability corresponding to time  $t > t_{\text{ref}}$ . Then  $t - t_{\text{ref}} = T_{\text{ref}} - T$  and equation (D3) can be rewritten as

$$V(T) = V_{\text{ref}} \exp \left[ \frac{T_{\text{ref}} - T}{t_a} - \frac{b}{a} \ln \left( 1 + \frac{T_{\text{ref}} - T}{\theta_{\text{ref}}} \right) \right]. \quad (\text{D4})$$

Because of stress step  $\Delta\tau$  at time  $t > t_{\text{ref}}$ , slip velocity abruptly increases to  $V(T) \exp[\Delta\tau/(a\bar{\sigma})]$  and, in this scenario,  $V\theta/L$  becomes much larger than 1. The new time to instability can be found from equation (B3):

$$\begin{aligned} f(T) = t_a \ln \left\{ 1 + \frac{\dot{\tau}}{H\bar{\sigma}V_{\text{ref}}} \right. \\ \left. \cdot \exp \left[ \frac{\dot{\tau}(T - T_{\text{ref}}) - \Delta\tau}{a\bar{\sigma}} + \frac{b}{a} \ln \left( 1 + \frac{T_{\text{ref}} - T}{\theta_{\text{ref}}} \right) \right] \right\}. \end{aligned} \quad (\text{D5})$$

Keeping only the term linear in  $T$  under the exponential, one can solve for  $T$  and calculate  $dT/df$  to obtain

$$\frac{R}{r} = \frac{1}{1 - \exp(-f/t_a)}. \quad (\text{D6})$$

For  $f \ll t_a$ , one has  $R/r = t_a/f$ , which shows a power law decay of the aftershock rate with the normalized time  $f/t_a$ . For  $f \gg t_a$ , one gets  $R/r = 1$  and the aftershock rate becomes the background rate.

### D3. Scenario 3: Nucleation Zones Close to Failure With $V\theta/L \sim 1$ Before the Perturbation and $V\theta/L \gg 1$ After the Perturbation

[95] In simulations with  $a/b \gtrsim 0.5$ , the value of  $V\theta/L$  becomes close to 1 for a large part of the nucleation zone shortly before the instability (section 5.2), consistently with the study of *Rubin and Ampuero* [2005]. This results in elevated aftershock rates in comparison to Dieterich's estimate (e.g., case 2 in Figure 8).

#### D3.1. Approach 1

[96] To approximately estimate the impact of  $V\theta/L \sim 1$  on aftershock rates, let us consider a nucleation process in the spring-slider model with  $V\theta/L = 1$  before the stress step. The governing equation becomes

$$\tau_{\text{ref}}^o - k\delta = \bar{\sigma} \left[ \mu_0 + (a - b) \ln \left( \frac{V}{V_0} \right) \right]. \quad (\text{D7})$$

Here we ignore the loading term  $\dot{\tau}t$ , considering a nucleation process that is so close to failure that it is beyond the influence of slow tectonic loading. Taking into account that  $\tau_{\text{ref}}^o - k\delta_{\text{ref}} = \bar{\sigma} [\mu_0 + (a - b) \ln (V_{\text{ref}}/V_0)]$  and solving for  $V$ , we obtain

$$V(t) = \frac{d\delta}{dt} = \frac{V_{\text{ref}}}{V_{\text{ref}} \hat{k}(t - t_{\text{ref}}) + 1}, \quad (\text{D8})$$

where  $\hat{k} = k/((a - b) \bar{\sigma})$ . As in section D2, we can rewrite this expression in terms of the original time to instability  $T$  (using  $t - t_{\text{ref}} = T_{\text{ref}} - T$ ), get slip velocity after the stress step as  $V(T) \exp[\Delta\tau/(a\bar{\sigma})]$ , and find the new time to instability corresponding to this slip velocity using equation (B4):

$$f(T) = \frac{a(V_{\text{ref}} \hat{k}(T_{\text{ref}} - T) + 1)}{HV_{\text{ref}} \exp(\Delta\tau/(a\bar{\sigma}))}. \quad (\text{D9})$$

Solving for  $T$  and calculating  $dT/df$ , we obtain

$$\frac{R}{r} = \left( \frac{(b - a)b\bar{\sigma}}{aLk} - \frac{(b - a)}{a} \right) \exp \left( \frac{\Delta\tau}{a\bar{\sigma}} \right). \quad (\text{D10})$$

[97] In equation (D10), aftershock rates right after the main shock are different from the model of *Dieterich* [1994] by the factor of  $[(b - a)b\bar{\sigma}/(aLk) - (b - a)/a]$ . To compare this result with our computed aftershock rates, we need to estimate the effective stiffness  $k$  of the simulated nucleation process which changes with time. Since we are considering the final stages of nucleation in this scenario, we set  $k = \eta G/h_{\text{nucl}}$ , where  $h_{\text{nucl}}$  is the nucleation size right before instability. Using expression (3) for  $h_{\text{nucl}}$  with  $F = (b - a)^2/b$  and  $\eta = 2/\pi$  found by *Rubin and Ampuero* [2005] for  $a/b$  close to 1, we get

$$\frac{R}{r} = \left( \frac{b^2}{2a(b - a)} - \frac{(b - a)}{a} \right) \exp \left( \frac{\Delta\tau}{a\bar{\sigma}} \right). \quad (\text{D11})$$

For case 2 (Figure 8), the simulated aftershock rates are larger by a factor of 3.8 relative to the model of *Dieterich* [1994], while the estimate (D11) predicts a factor of 2.7.

### D3.2. Approach 2

[98] Instead of using the unperturbed slip velocity history (D8), let us assume that the nucleation process follows the behavior given by equation (44) of *Rubin and Ampuero* [2005] for quasi-static nucleation with  $a/b$  close to 1:

$$T = \frac{2}{\pi} \frac{bL}{(b - a)V}. \quad (\text{D12})$$

Continuing with the same steps as in approach 1, we obtain

$$\frac{R}{r} = \left( \frac{2b^2}{\pi a(b - a)} - \frac{4(b - a)}{\pi a} \right) \exp \left( \frac{\Delta\tau}{a\bar{\sigma}} \right). \quad (\text{D13})$$

For case 2 (Figure 8), this estimate gives 3.5 for the factor of aftershock rate increase relative to the model of *Dieterich* [1994], which is very close to the actual factor of 3.8.

[99] **Acknowledgments.** This study was supported by the Southern California Earthquake Center and by the National Science Foundation (grant EAR 0548277). SCEC is funded by NSF Cooperative Agreement EAR-0106924 and USGS Cooperative Agreement 02HQAG0008. We thank Yue Tian and Alan Rubin for giving permission to use their figures and for providing digital copies of them. We also thank Joan Gomberg, Alan Rubin, Paul Segall, and anonymous reviewers for helpful comments. This is SCEC contribution 1102.

### References

- Ampuero, J.-P., and A. M. Rubin (2008), Earthquake nucleation on rate and state faults: Aging and slip laws, *J. Geophys. Res.*, *113*, B01302, doi:10.1029/2007JB005082.
- Bayart, E., A. M. Rubin, and C. Marone (2006), Evolution of fault friction following large velocity jumps, *Eos Trans. AGU*, *87*(52), Fall Meet. Suppl., Abstract S31A-0180.
- Belardinelli, M. E., M. Cocco, O. Coutant, and F. Cotton (1999), Redistribution of dynamic stress during coseismic ruptures: Evidence for fault interaction and earthquake triggering, *J. Geophys. Res.*, *104*, 14,925–14,945.
- Benioff, H. (1951), Earthquakes and rock creep, *Bull. Seismol. Soc. Am.*, *41*, 31–62.
- Ben-Zion, Y., and V. Lyakhovsky (2006), Analysis of aftershocks in a lithospheric model with seismogenic zone governed by damage rheology, *Geophys. J. Int.*, *165*, 197–210, doi:10.1111/j.1365-246X.2006.02878.x.
- Ben-Zion, Y., and J. R. Rice (1997), Dynamic simulations of slip on a smooth fault in an elastic solid, *J. Geophys. Res.*, *102*, 17,771–17,784.
- Blanpied, M. L., D. A. Lockner, and J. D. Byerlee (1995), Frictional slip of granite at hydrothermal conditions, *J. Geophys. Res.*, *100*, 13,045–13,064.
- Bosl, W. J., and A. Nur (2002), Aftershocks and pore fluid diffusion following the 1992 Landers earthquake, *J. Geophys. Res.*, *107*(B12), 2366, doi:10.1029/2001JB000155.
- Daniel, G., D. Marsan, and M. Bouchon (2008), Earthquake triggering in southern Iceland following the June 2000  $M_s$  6.6 doublet, *J. Geophys. Res.*, *113*, B05310, doi:10.1029/2007JB005107.
- Dieterich, J. H. (1978), Time-dependent friction and the mechanics of stick-slip, *Pure Appl. Geophys.*, *116*, 790–806.
- Dieterich, J. H. (1979), Modeling of rock friction: 1. Experimental results and constitutive equations, *J. Geophys. Res.*, *84*, 2161–2168.
- Dieterich, J. H. (1992), Earthquake nucleation on faults with rate- and state-dependent strength, *Tectonophysics*, *211*, 115–134.
- Dieterich, J. H. (1994), A constitutive law for rate of earthquake production and its application to earthquake clustering, *J. Geophys. Res.*, *99*, 2601–2618.
- Dieterich, J. H., and B. D. Kilgore (1994), Direct observation of frictional contacts: New insights for state-dependent properties, *Pure Appl. Geophys.*, *143*, 283–302.
- Dieterich, J. H., and B. D. Kilgore (1996), Implications of fault constitutive properties for earthquake prediction, *Proc. Natl. Acad. Sci. U.S.A.*, *93*, 3787–3794.
- Felzer, K. R., and E. E. Brodsky (2006), Decay of aftershock density with distance indicates triggering by dynamic stress, *Nature*, *441*, 735–738.
- Freed, A. M., and J. Lin (2001), Delayed triggering of the 1999 Hector Mine earthquake by viscoelastic stress transfer, *Nature*, *411*, 180–183.

- Gomberg, J. (2001), The failure of earthquake failure models, *J. Geophys. Res.*, *106*, 16,253–16,263.
- Gomberg, J., N. M. Beeler, M. L. Blanpied, and P. Bodin (1998), Earthquake triggering by transient and static deformations, *J. Geophys. Res.*, *103*, 24,411–24,426.
- Gomberg, J., N. M. Beeler, and M. L. Blanpied (2000), On rate-state and Coulomb failure models, *J. Geophys. Res.*, *105*, 7857–7871.
- Gomberg, J., P. Bodin, and P. A. Reasenberg (2003), Observing earthquakes triggered in the near field by dynamic deformations, *Bull. Seismol. Soc. Am.*, *93*, 118–138.
- Gomberg, J., P. Reasenberg, M. Cocco, and M. E. Belardinelli (2005), A frictional population model of seismicity rate change, *J. Geophys. Res.*, *110*, B05S03, doi:10.1029/2004JB003404.
- Gross, S., and R. Burgmann (1998), Rate and state of background stress estimated from the aftershocks of the 1989 Loma Prieta, California, earthquake, *J. Geophys. Res.*, *103*, 4915–4927.
- Gross, S., and C. Kisslinger (1997), Estimating tectonic stress rate and state with Landers aftershocks, *J. Geophys. Res.*, *102*, 7603–7612.
- Gu, J. C., J. R. Rice, A. L. Ruina, and S. T. Tse (1984), Slip motion and stability of a single degree of freedom elastic system with rate and state dependent friction, *J. Mech. Phys. Solids*, *32*, 167–196.
- Hill, D. P. (1993), Seismicity remotely triggered by the magnitude 7.3 Landers, California, earthquake, *Science*, *260*, 1617–1623.
- Kato, N., and T. E. Tullis (2001), A composite rate- and state-dependent law for rock friction, *Geophys. Res. Lett.*, *28*(6), 1103–1106.
- Lapusta, N. (2001), Elastodynamic analysis of sliding with rate and state friction, Ph.D. Thesis, Div. of Eng. and Appl. Sci., Harvard Univ., Cambridge, Mass.
- Lapusta, N., and J. R. Rice (2002), Nucleation of rate and state frictional instability under non-uniform loading, *Eos Trans. American Geophysical Union*, *83*(47), Fall Meet. Suppl., Abstract S61E-05.
- Lapusta, N., and J. R. Rice (2003), Nucleation and early seismic propagation of small and large events in a crustal earthquake model, *J. Geophys. Res.*, *108*(B4), 2205, doi:10.1029/2001JB000793.
- Lapusta, N., J. R. Rice, Y. Ben-Zion, and G. Zheng (2000), Elastodynamic analysis for slow tectonic loading with spontaneous rupture episodes on faults with rate- and state-dependent friction, *J. Geophys. Res.*, *105*, 23,765–23,789.
- Lehner, F. K., V. C. Li, and J. R. Rice (1981), Stress diffusion along rupturing plate boundaries, *J. Geophys. Res.*, *86*, 6155–6169.
- Liu, Y., and J. R. Rice (2005), Aseismic slip transients emerge spontaneously in 3D rate and state modeling of subduction earthquake sequences, *J. Geophys. Res.*, *110*, B08307, doi:10.1029/2004JB003424.
- Marone, C. (1998), Laboratory-derived friction laws and their application to seismic faulting, *Annu. Rev. Earth Planet. Sci.*, *26*, 643–696.
- Marone, C. J., C. H. Scholz, and R. Bilham (1991), On the mechanics of earthquake afterslip, *J. Geophys. Res.*, *96*, 8441–8452.
- Miyazaki, S., P. Segall, J. J. McGuire, T. Kato, and Y. Hatanaka (2006), Spatial and temporal evolution of stress and slip rate during the 2000 Tokai slow earthquake, *J. Geophys. Res.*, *111*, B03409, doi:10.1029/2004JB003426.
- Nur, A., and J. R. Booker (1972), Aftershocks caused by pore fluid flow?, *Science*, *175*, 885–887.
- Perfettini, H., and J.-P. Avouac (2004), Postseismic relaxation driven by brittle creep: A possible mechanism to reconcile geodetic measurements and the decay rate of aftershocks, application to the Chi-Chi earthquake, Taiwan, *J. Geophys. Res.*, *109*, B02304, doi:10.1029/2003JB002488.
- Perfettini, H., J. Schmittbuhl, and A. Cochard (2003), Shear and normal load perturbations on a two-dimensional continuous fault: 1. Static triggering, *J. Geophys. Res.*, *108*(B10), 2408, doi:10.1029/2002JB001804.
- Rice, J. R. (1993), Spatio-temporal complexity of slip on a fault, *J. Geophys. Res.*, *98*, 9885–9907.
- Rice, J. R., and Y. Ben-Zion (1996), Slip complexity in earthquake fault models, *Proc. Natl. Acad. Sci. U. S. A.*, *93*, 3811–3818.
- Rice, J. R., and A. L. Ruina (1983), Stability of steady frictional slipping, *J. Appl. Mech.*, *50*, 343–349.
- Rice, J. R., N. Lapusta, and K. Ranjith (2001), Rate and state dependent friction and the stability of sliding between elastically deformable solids, *J. Mech. Phys. Solids*, *49*, 1865–1898.
- Rubin, A. M., and J.-P. Ampuero (2005), Earthquake nucleation on (aging) rate and state faults, *J. Geophys. Res.*, *110*, B11312, doi:10.1029/2005JB003686.
- Ruina, A. L. (1983), Slip instability and state variable friction laws, *J. Geophys. Res.*, *88*, 10,359–10,370.
- Schaff, D. P., G. H. R. Bokelmann, G. C. Beroza, F. Waldhauser, and W. L. Ellsworth (2002), High-resolution image of Calaveras Fault seismicity, *J. Geophys. Res.*, *107*(B9), 2186, doi:10.1029/2001JB000633.
- Schwartz, S. Y., and J. M. Rokosky (2007), Slow slip events and seismic tremor at circum-Pacific subduction zones, *Rev. Geophys.*, *45*, RG3004, doi:10.1029/2006RG000208.
- Tian, Y., and A. M. Rubin (2005), Abrupt turnoff of aftershocks after a major earthquake, paper presented at Chapman Conference on Radiated Energy and the Physics of Earthquake Faulting, AGU, Portland, Maine, 13–17 June.
- Toda, S., R. S. Stein, P. A. Reasenberg, J. H. Dieterich, and A. Yoshida (1998), Stress transferred by the 1995  $M_w = 6.9$  Kobe, Japan, shock: Effect on aftershocks and future earthquake probabilities, *J. Geophys. Res.*, *103*, 24,543–24,565.
- Toda, S., R. S. Stein, K. Richards-Dinger, and S. B. Bozkurt (2005), Forecasting the evolution of seismicity in southern California: Animations built on earthquake stress transfer, *J. Geophys. Res.*, *110*, B05S16, doi:10.1029/2004JB003415.
- Tullis, T. E. (1988), Rock friction constitutive behavior from laboratory experiments and its implications for an earthquake prediction field monitoring program, *Pure Appl. Geophys.*, *126*, 555–588.
- Tullis, T. E. (1996), Rock friction and its implications for earthquake prediction examined via models of Parkfield earthquakes, *Proc. Natl. Acad. Sci. U. S. A.*, *93*, 3803–3810.
- Utsu, T., Y. Ogata, and R. S. Matsu'ura (1995), The centenary of the Omori formula for a decay law of aftershock activity, *J. Phys. Earth*, *43*, 1–33.
- Waldhauser, F., W. L. Ellsworth, D. P. Schaff, and A. Cole (2004), Streaks, multiplets, and holes: High-resolution spatio-temporal behavior of Parkfield seismicity, *Geophys. Res. Lett.*, *31*, L18608, doi:10.1029/2004GL020649.

Y. Kaneko and N. Lapusta, Division of Geological and Planetary Sciences, California Institute of Technology, Pasadena, CA 91125, USA. (ykaneko@gps.caltech.edu; lapusta@caltech.edu)